FNAL- TD-06-062; LARP-SRD-02

Editor: Giorgio Ambrosio
Fermi National Accelerator Laboratory
Technical Division
Magnet System Department
Mail stop 315
P.O. Box 500
Batavia, Illinois • 60510

TD-06-062
LARP_SRDnote_02
11/13/2006

DESIGN OF THE FIRST LARP LONG RACETRACK MAGNET (LRS01)

G. Ambrosio[1], M. Anerella[2], E. Barzi[1], D. Cheng[3], D. Dietderich[3], P. Ferracin[3], A. Ghosh[2], S. Gourlay[3], R. Hafalia[3], A Lietzke[3], A. McInturff[4], J. Muratore[2], F. Nobrega[1], G.L. Sabbi[3], J. Schmalzle[2], P. Wanderer[2], A.V. Zlobin[1]

Editor: G. Ambrosio[1]

[1]Fermi National Accelerator Laboratory, Batavia IL 60510, USA
[2]Brookhaven National Laboratory, Upton NY 11973, USA
[3]Lawrence Berkeley National Laboratory, Berkeley CA 94720, USA
[4]LBNL and Texas A&M University, College Station, Texas 77843, USA

Abstract:

The LHC Accelerator Research Program (LARP) is developing, Nb_3Sn quadrupole magnet models for a luminosity upgrade of the Large Hadron Collider (LHC). A major milestone in this development is to assemble and test two 4m-long quadrupole cold masses by the summer of 2009.

These quadrupole magnets will be the first Nb_3Sn accelerator magnet models significantly longer than 1m, approaching the length of real accelerator magnets. The design is based on the LARP Technological Quadrupoles (TQ), with gradient higher than 200 T/m and aperture of 90 mm, made of two layers without interlayer splice. The mechanical design will be chosen between two designs presently explored for the TQs: traditional collars and Al-shell based design (preloaded by bladders and keys).

The fabrication of the first long quadrupole model is expected to start in the last quarter of 2007. Before that 4m-long racetrack coils will be fabricated and tested in an Al-shell based supporting structure. They will allow a quick start in addressing several issues related with the fabrication of long Nb_3Sn coils. The design of the first Long Racetrack magnet (LRS01), including conductor and insulation features, quench protection studies and the supporting structure is presented in this report.

TABLE OF CONTENTS

1. INTRODUCTION

2. CONDUCTOR CHARACTERISTICS
By A. Ghosh

3. MAGNETIC DESIGN
By P. Ferracin

4. COIL FEATURES AND FABRICATION
By J. Schmalzle, and D. Dietderich

5. MECHANICAL DESIGN
By P. Ferracin, D. Cheng, and R. Hafalia

6. MAGNET ASSEMBLY
By D. Cheng, R. Hafalia, P. Ferracin, and J. Schmalzle

7. QUENCH PROTECTION
By J. Muratore

8. COIL INSTRUMENTATION
By G. Ambrosio, and P. Wanderer

References

1. INTRODUCTION

The goal of the LARP Long Racetracks is to provide a reliable test bed for the fabrication and test of long Nb_3Sn coils before starting the fabrication of the LARP Long Quadrupole.

The design of the first LARP Long Racetrack (LRS01) is based on the design of the small racetracks (SM series) developed at LBNL [1.1]. In the SM two double-layer 30.5-cm long racetrack coils are connected in a common-coil configuration so that the largest component of the magnetic forces tries to separate the two double-layers, and only small forces are acting in the other directions. The coil separation is constrained by an aluminum shell preloaded using bladders and keys.

This concept, successfully adopted in several small racetracks [1.2], is here adopted for the first time for the fabrication and test of 3.6-m long coils. The significantly larger length of LRS01 required a few modifications to the SM design: thicker coil skins, larger yoke diameter, larger gap for the extraction of bladders, use of side-rails and end-saddle instead of the SM horse-shoe, iron island longitudinally split into 5 parts, additional cloth to increase the layer-to-layer insulation strength, use of strip heaters for magnet quench protection.

The details of magnet design and assembly procedure are described in the following.

2. CONDUCTOR CHARACTERISTICS

a. Strand Characteristics

The cable for LRS magnets will be fabricated using the Rod-Restack Process (RRP) wire from Oxford-Instruments Superconducting Technology (OI-ST). Strand diameter is nominally 0.7mm and is of the 54/61 design. The minimum strand requirements are specified in the LARP conductor specification LARP-MAG-M-8001-RevB. Initial acceptance tests show that the wires from billet 8647 and 8648 meet the critical current and RRR requirements. The average Cu/non-Cu ratio of the strands is 0.87 and when reacted at 650C/48hrs has a RRR greater than 200. Low field stability measurements show that strands reacted with the following schedule (used for strand acceptance): 48hrs/210C + 48hrs/400C + 48hrs/650C have a minimum I_s of 975A. These tests have only been done at BNL. Tests are also being done at FNAL and will be available shortly. Once cable has been fabricated, the heat-treatment will be optimized for extracted strands to ensure both a minimum I_c, and I_s.

b. Cable Characteristics

The rectangular cable fabricated will use 20 strands and have a minimum length of 350 m. For this program the plan is to initially manufacture 3 unit lengths of cable. Each cable run will require 26 kg of wire with UL's of 380m. The detailed cabling map will be drawn-up by LBNL before cable manufacture. After cabling, it will be annealed for 8 hrs at 200C and subsequently re-rolled to the following dimensions, width: 7.793 ± 0.050 mm, mid-thickness: 1.276 ± 0.010 mm.

Samples of cable will be tested at FNAL using the transformer method to determine the self-field quench currents. This will establish the minimum stability current for the cable. Cable tests will be preceded by extracted strand tests to optimize the reaction schedule.

3. MAGNETIC DESIGN

a. Magnet parameters

The magnet's parameters are given in Table I. Magnet short sample computations have been performed assuming a J_c in the superconductor of 2800 A/mm^2 at 4.2 K and 12 T (Summers' formula). The Jc assumption is consistent with preliminary strand measurements performed at BNL (Fig. 3.1).

b. 2D Magnetic Model

The field in the conductor has been computed by a 2D magnetic model of the magnet cross-section (Fig. 3.2), where each individual turn has been considered. The highest field of 12.23 T (Fig. 3.3) is located in the inner surface of the coil (facing the *y* axis), approximately between turn 10 and turn 12 (counting from the island).

c. 3D Magnetic Model

In Fig. 3.4 we show the 3D magnetic model. To reduce the CPU time, we reduced the total length of the coil straight section to about 300 mm (twice as long as the current short subscale coils). In Fig. 3.5 and Fig. 3.6 we show the field in the conductor at short sample. The peak field is located in the center of the coil, approximately in turn 11 (as already observed in the 2D model). The different between the peak field computed in the 2D model (12.23 T) and in the 3D model (12.19 T) is of 0.04 T (Fig. 3.7). In Fig. 3.8 the field variation along the straight section is plotted: from the maximum of 12.19 T in the center, the field decreases to 11.60 T at the end of the straight section. In the end region, the field further decreases to 11.00 T (Fig. 3.9).

The longitudinal Lorentz force at short sample is of 40 kN per coil.

Table I
Magnet parameters

Parameter	**Unit**	
Cable type		SM
N° of double-layer coils		2
Number of turns per layer		21
Strand diameter	mm	0.700
Number of strands		20
Conductor volume	Kg/m	
Cable width (bare)	mm	7.793
Cable thickness (bare)	mm	1.275
Insulation thickness	mm	0.092
Cu/Sc ratio		0.90
J_c(12 T,4.2 K)	A/mm^2	2800
B_{peak}(4.2 K)	T	12.23
I_{ss} (4.2 K)	kA	10.80
I_{ss} (4.2 K) per strand	A	540
Inductance @ I_{ss} (4.2 K)	mH/m	1.5
Energy @ I_{ss} (4.2 K)	kJ/m	86
F_x per quadrant @ I_{ss}	kN/m	+1903
F_y per quadrant @ I_{ss}	kN/m	-9
F_z per quadrant @ I_{ss}	kN	20

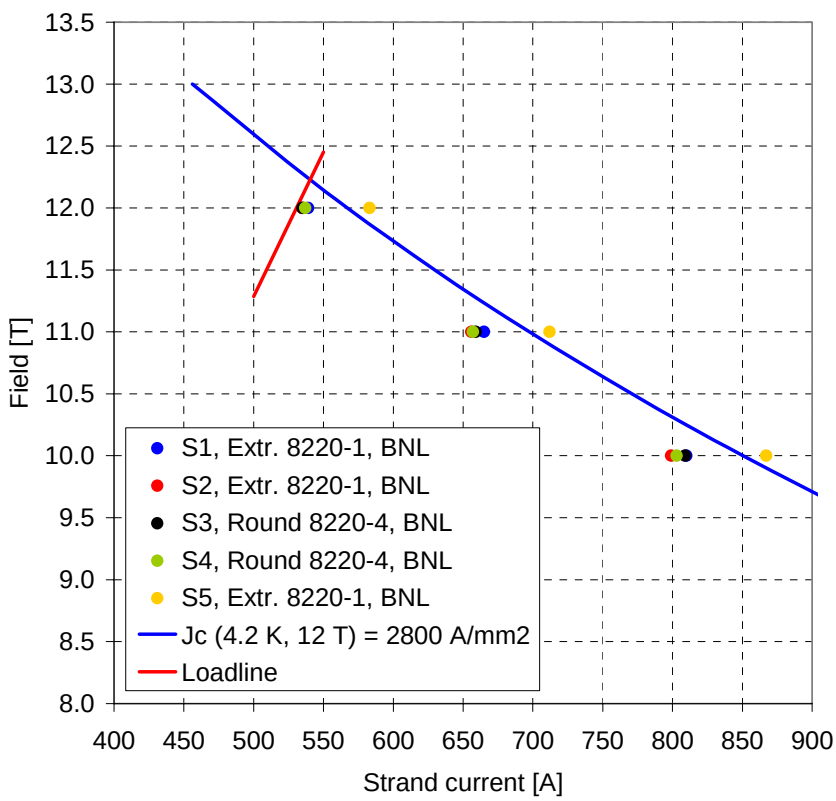

Fig. 3.1: Magnet loading line compared with strand measurements and Summers' parameterization (right).

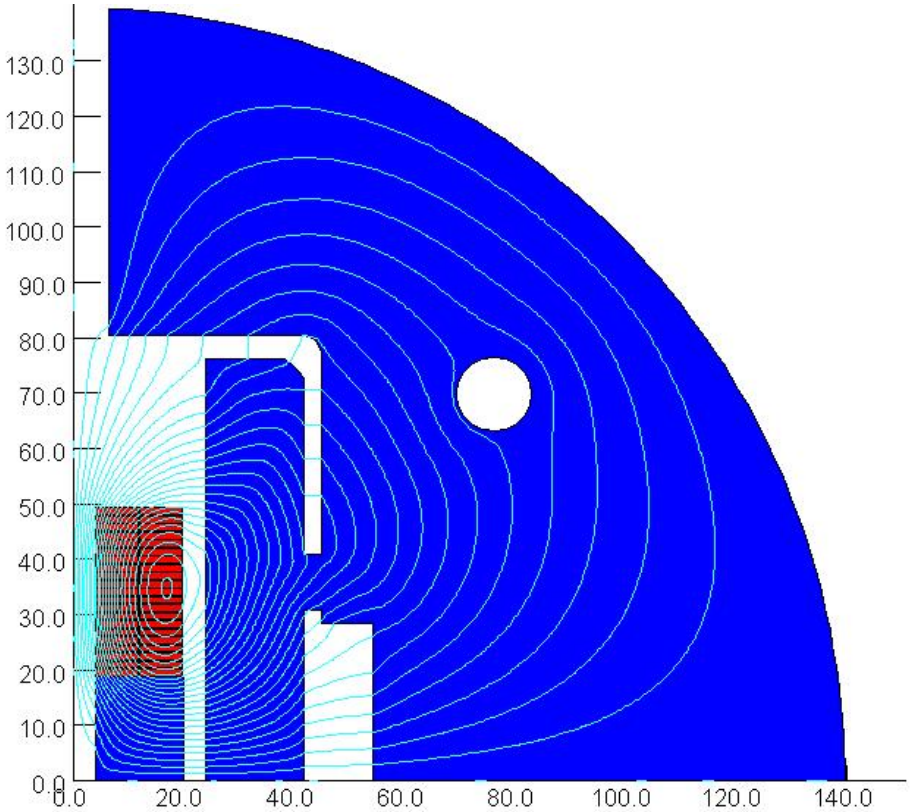

Fig. 3.2: Flux line computed by the 2D magnetic model.

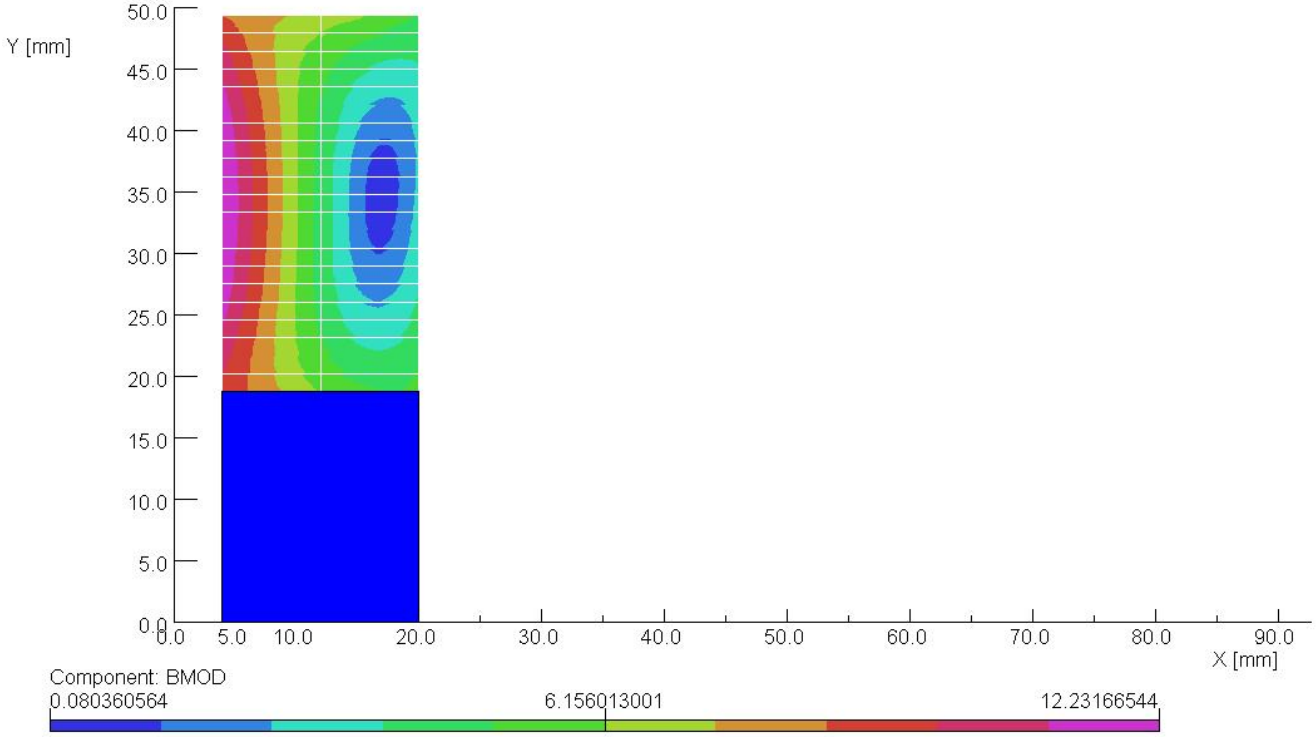

Fig. 3.3: Magnetic field (T) in the conductor at short sample (10.80 kA).

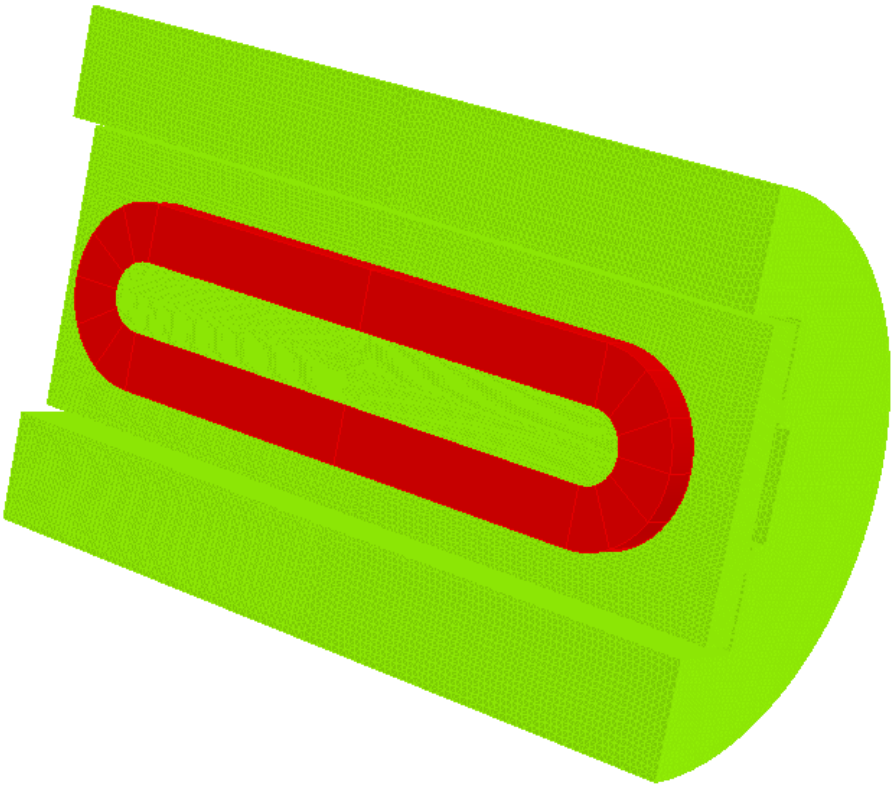

Fig. 3.4: 3D magnetic model.

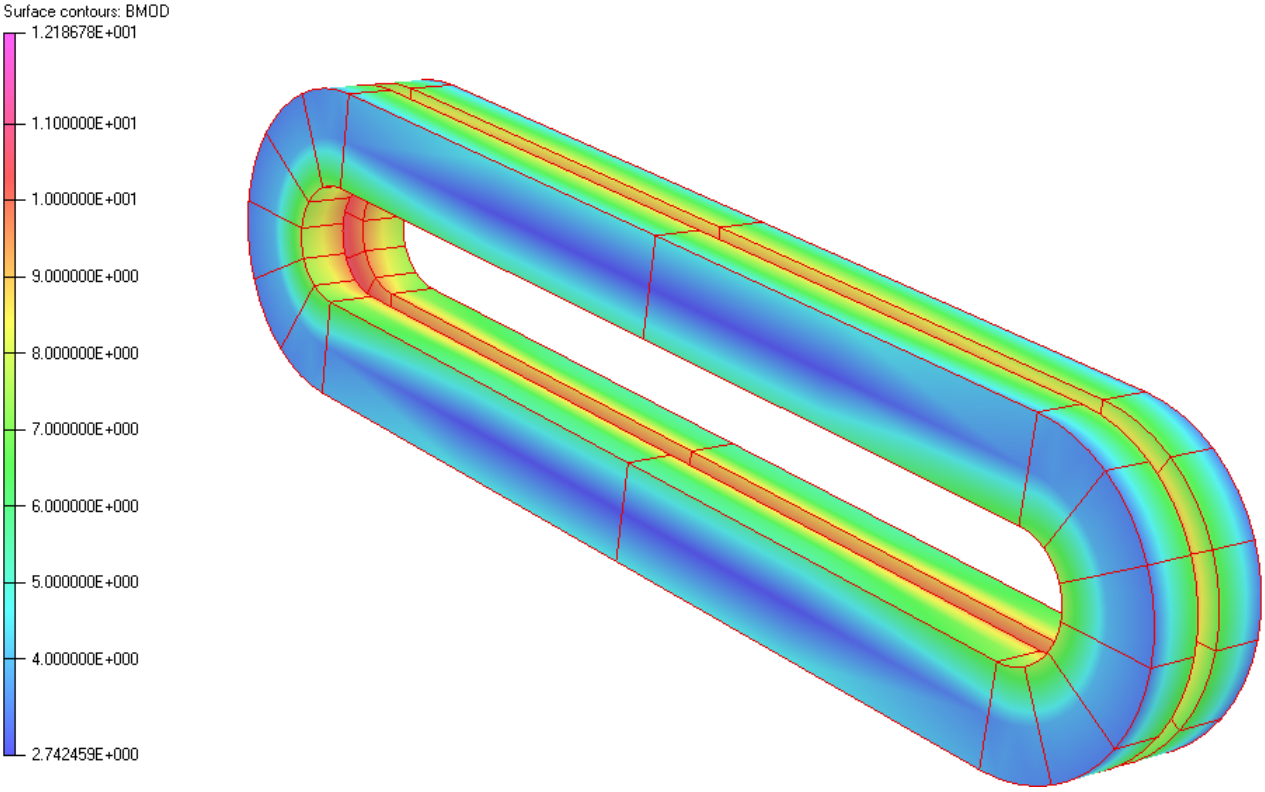

Fig. 3.5: Magnetic field (T) in the conductor (outer surface) at short sample (10.80 kA).

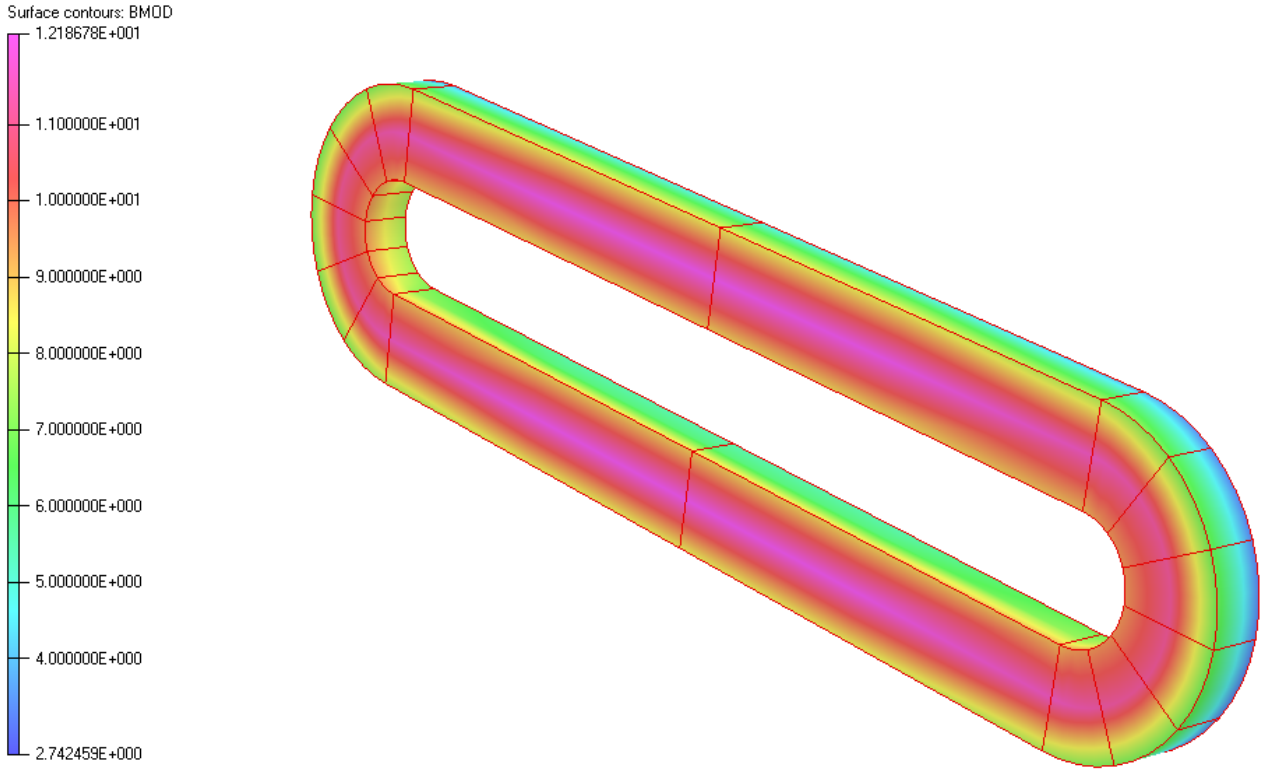

Fig. 3.6: Magnetic field (T) in the conductor (inner surface) at short sample (10.80 kA).

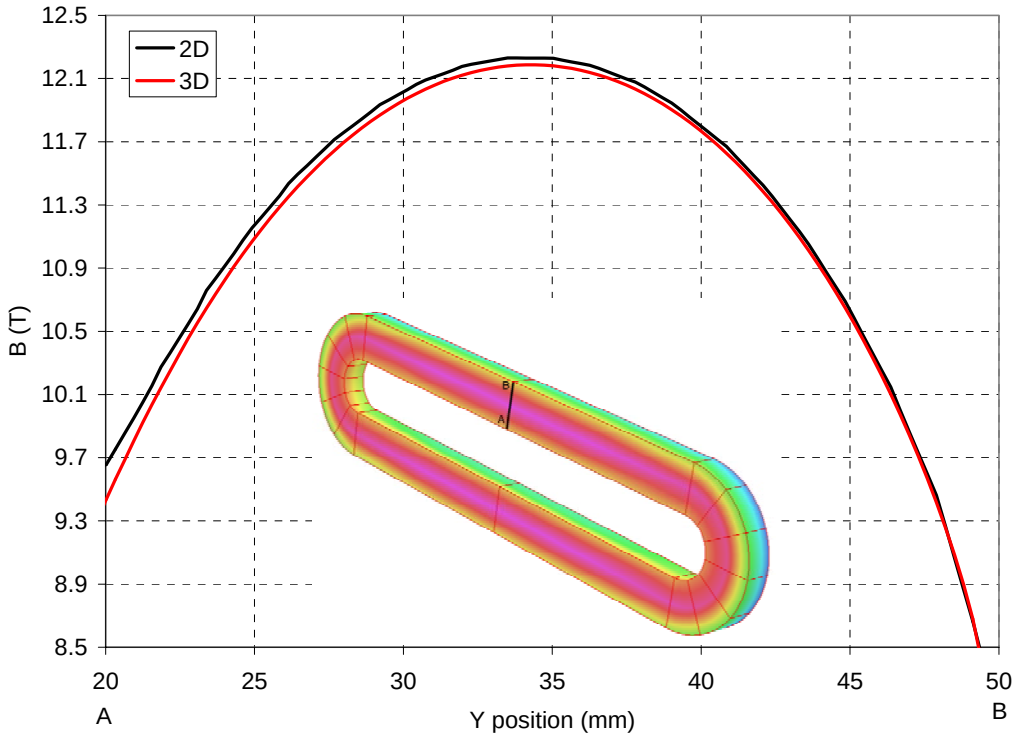

Fig. 3.7: Magnetic field (T) in the conductor at short sample (10.80 kA): comparison between 2D and 3D models.

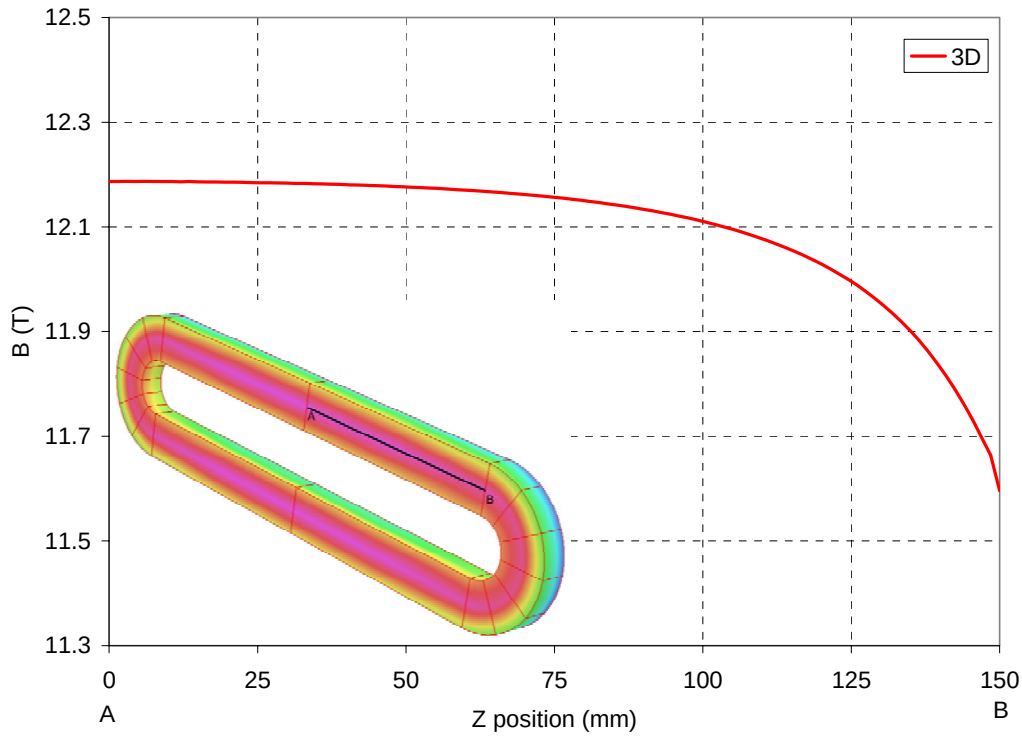

Fig. 3.8: Magnetic field (T) in the conductor at short sample (10.80 kA): path along the straight section.

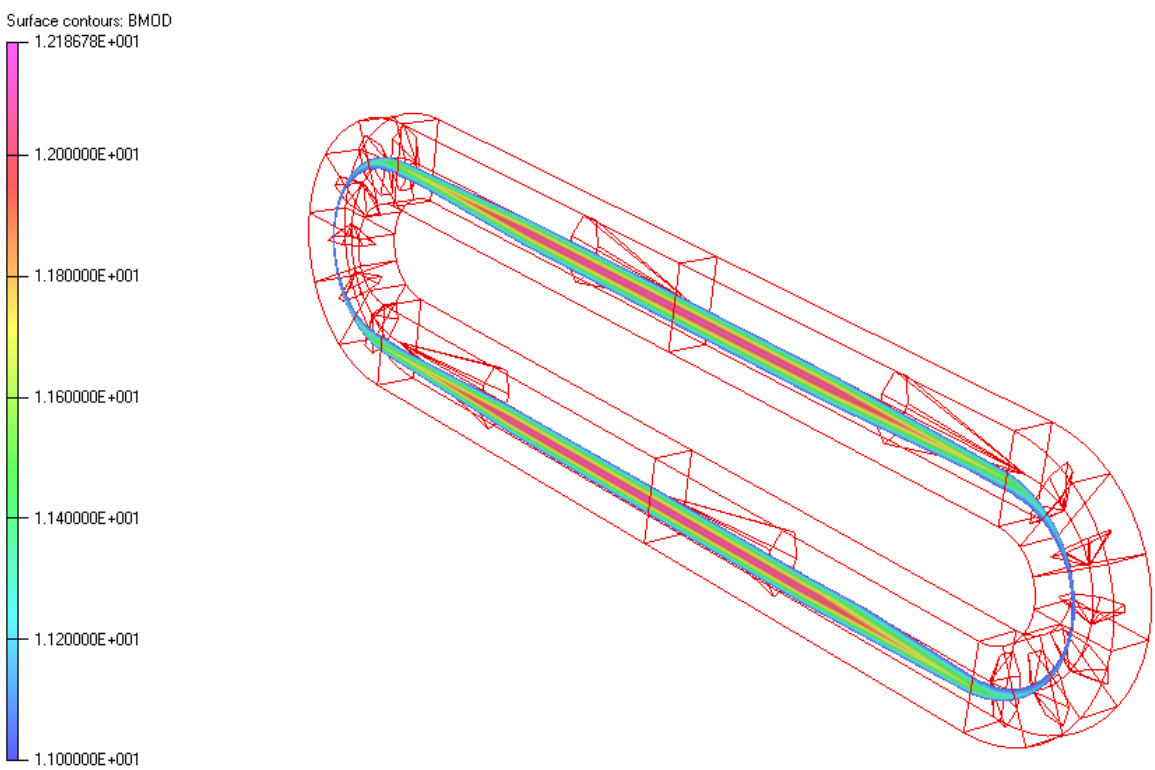

Fig. 3.9: Magnetic field (T) in the conductor at short sample (10.80 kA): difference between straight section and ends.

4. COIL FEATURES AND FABRICATION

a. Cable Insulation

The cable insulation procedure is described in the following with real numbers measured during the insulation of a TQ cable. The insulation is an S-glass sleeve 0.092 mm thick (after application on a cable). The length of the unit used in this example was 762m (2500 ft.).

- "762m" of sleeve weighed 4.450kg. (171.2m/kg)

- Re-spooled onto a stainless spool and heat cleaned at 850F/2hr.
    - After cleaning "762m" weighed 3.121kg. (244.1m/kg)
    - Cleaning removed 1.329kg organic material. (30%)

- Palmitic acid sizing was applied to the cleaned glass by passing the sleeve through a Palmitic-acid/Ethanol solution.
    - 100g Palmitic-Acid
    - 2,000g Ethanol, heated and stirred at 35c.
    - 3m Vertical drying column at 48c
    - Insulation drawn through solution and drying column ~ 1m/min.
    - 200m Cleaned weighed 0.820kg.
    - 200m Treated weighed 0.827kg. (241.8m/kg) = 0.93% by weight Palmitic-Acid.

- "200m" Treated insulation was then slid over ~11m length of TFE tubing with cable inside.
- Cable was then slid through stationary TFE tube and treated insulation slid on to cable.
- "200m" treated glass insulation covered 169.5m of cable with ~2m remaining.
    - Insulation to cable ratio is 198/169.5 (1.17insulation:1cable)

b. Coil Features and Fabrication

The long racetrack coil design is intended to closely match that of the short racetrack coil, with changes made only as required by issues associated with the increased length. Each coil (Fig 4.1) is a double layer pancake made from a single length of cable with no interlayer splice. The transition of the cable between layers occurs at the lead end pole tip. The pole island surface which contacts the cable is insulated with a plasma spray coating of Aluminum Oxide. The island is segmented to allow for the release of cable tension built up during winding and to establish gaps before reaction that will allow for the differential expansion / contraction between the cable and the island during the reaction cycle. The coil has an end saddle at each end and full length stainless steel rails on each side.

Coil Features Table:

Pole width	37.19 mm (1.464 in.)
Aluminum oxide island coating thickness	0.30 mm (.012 in.)
Coil straight section length	3.45 m (136 in.)
Coil overall length	3.61 m (142 in.)
Island material	Iron
Number of island segments	5
Island gap size prior to reaction	0.42mm/m minimum
Cable insulation	Fiberglass sock

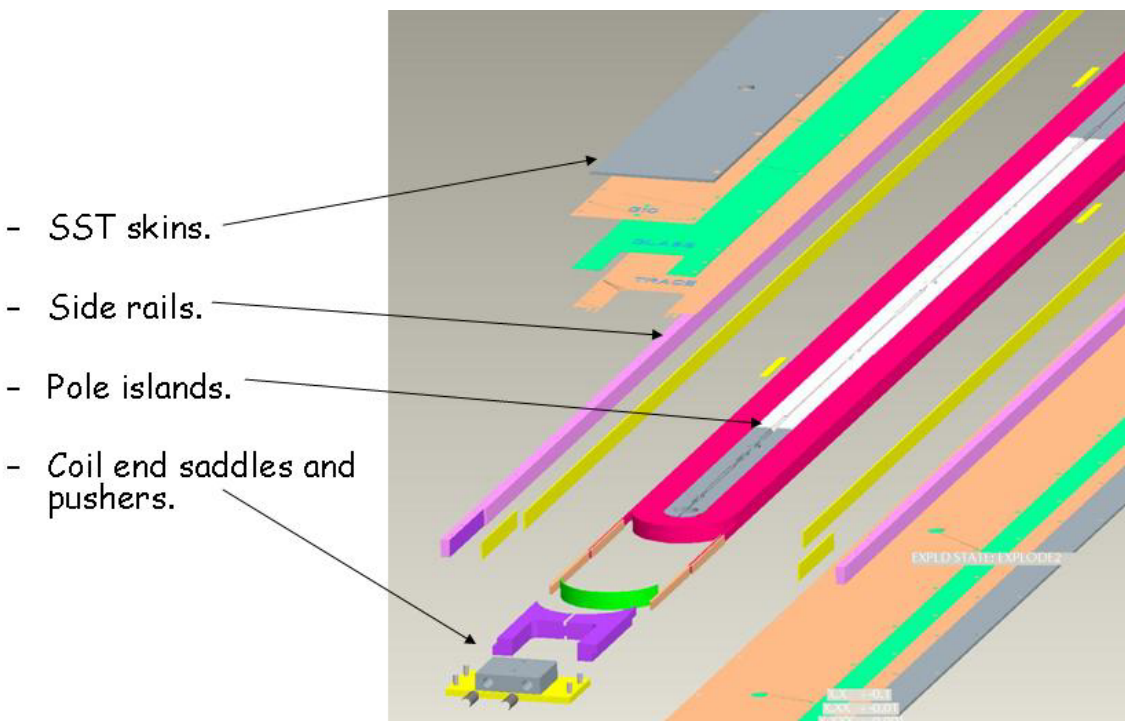

Fig. 4.1: Coil parts

The fabrication process begins with the re-spooling of cable onto winding spools. During this process the insulated cable is vacuumed and checked for debris using a lump detector. When completed the cable is divided between two spools, one which is installed onto the winding machine carriage for winding of the first layer and the other which is mounted above the coil pole island for use on the second layer. The coil is wound using a semi-automatic computer controlled winding machine with pneumatic clamps. To maintain proper coil configuration, the coil is wound with 25 lbs tension,

and the coil is clamped one side at a time while the opposite side is wound. After winding the coil is bolted into the reaction tooling and loaded to a coil stress of approximately 1000 psi in the direction normal to the face of the cable. Reaction takes place in a gas tight oven using an automatic program following the cycle shown in figure 4.2. A continuously flowing argon atmosphere is used to carry away any contaminates that are released during the reaction cycle. An argon flow rate of 25 cfh will be used until 400 C is reached. At that point all the palmitic acid will have been vaporized and the flow rate will be reduced to 10 cfh. Following reaction the coil is transferred to the impregnation tooling, the instrumentation / quench heater traces are installed and stabilizers are soldered to the leads. Coils are then hung vertically in a vacuum tank, impregnated with CTD 101K epoxy and cured using an automatic cycle as shown in figure 4.3. After impregnation the coil is inspected, electrical tests are performed, layers of insulation are added and both faces are covered with stainless steel skins that are bolted to the side rails. See following table for stack up summary.

A practice coil will be made of copper cable in order to test the automatic winding machine. The practice coil will then be impregnated to prove out the impregnation tooling and procedure.

Coil Stack up Table:

Item	**Thickness mm (in.)**
Impregnated Coil	17.22 (.678)
Fiberglass Cloth	0.25 (.010)
Instrumentation / Heater Trace	0.18 (.007)
Coil (island height)	16.36 (.644)
Instrumentation / Heater Trace	0.18 (.007)
Fiberglass Cloth	0.25 (.010)
Assembly Stack Up – starting at center	24.19 (.953)
Mylar	0.04 (.0015)
G10 / Kapton	0.13 (.005)
Stainless steel skin	3.18 (.125)
G10 / Kapton	0.13 (.005)
Impregnated Coil	17.22 (.678)
G10 / Kapton	0.13 (.005)
Stainless steel skin	3.18 (.125)
Mylar	0.08 (.003)
G10 / Kapton	0.13 (.005)

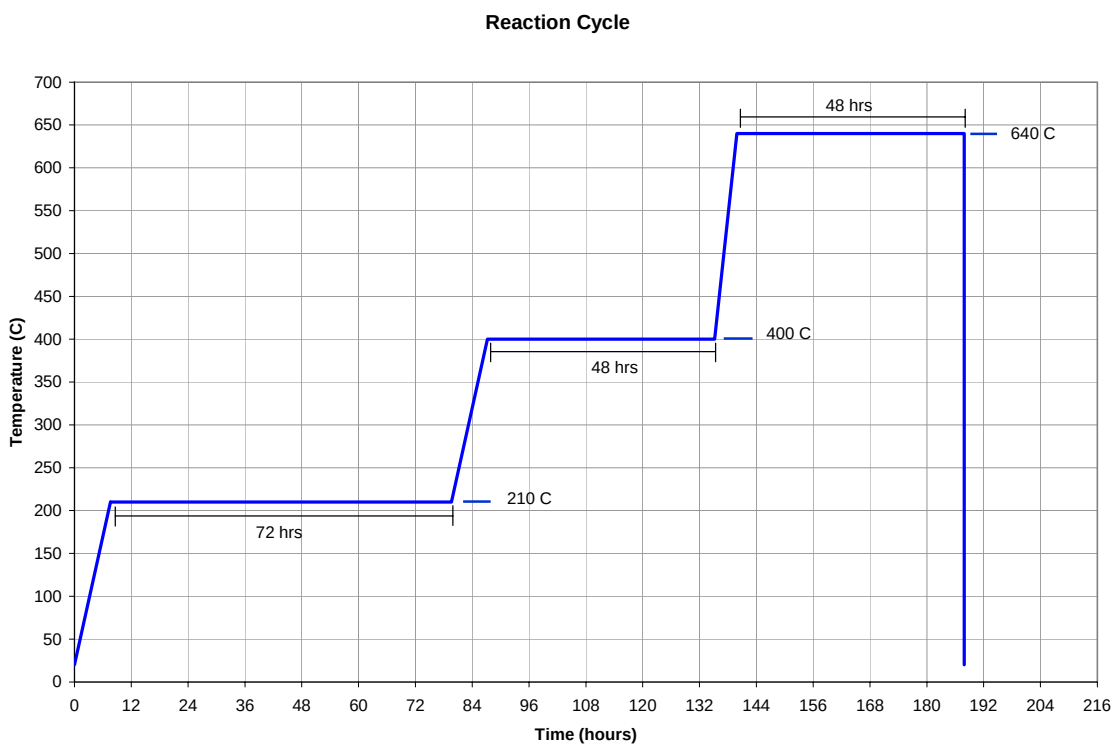

Fig. 4.2: Reaction cycle

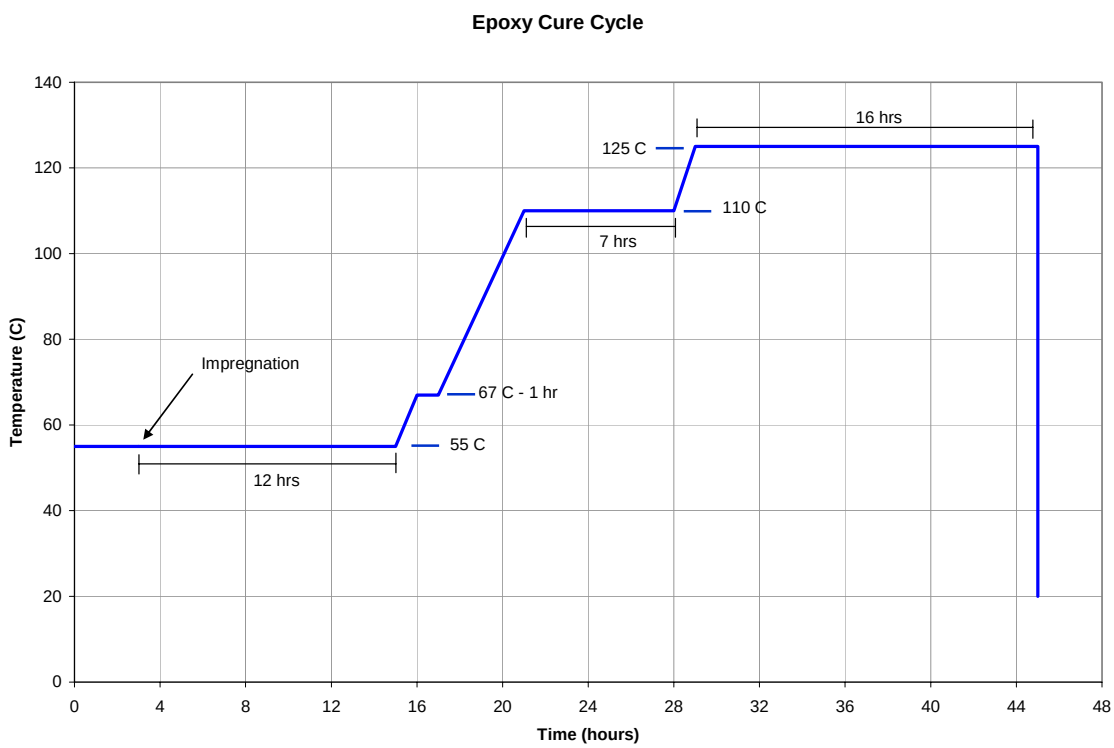

Fig. 4.3: Epoxy curing cycle

c. Reaction tooling stress relieving

In order to ensure straightness of the coil reaction fixture it is our intension to stress relieve the top, bottom, and side plates during the machining sequence as follows:

- The raw material (347H stainless) is solution heat treated as received.
- It will be rough machined at BNL then sent out for stress relieving to remove stresses caused by the machining operations. Stress relieving will be achieved via a soak at 1500-1600 F for 1 hour followed by air cooling.
- After stress relieving the parts will be ground to final flatness and straightness tolerances of .005 in/ft before machining of keyways, holes, etc.
- The parts will be inspected after grinding to ensure that they meet flatness and straightness tolerances as received from grinding and again after all final secondary machining operations.
- The completed fixture will then be assembled on the coil prep station and inspected to document flatness.
- The fixture will then be subjected to a typical coil reaction cycle. After the reaction cycle the fixture will be returned to the coil prep station and again inspected to verify that it still meets flatness tolerances.

d. Impregnation checks:

We want to be certain that the impregnation procedure is optimal.

Presently, we are doing a few test impregnations in our round test coil potting fixture in order to finalize the impregnation procedure in time for the 4m long LARP coils. These are intended to be quick-turnaround tests. The fixture is small and the coils are easily hand-insulated and hand-wound. Plus, clean-up is minimal. This fixture was used successfully for similar tests during the common coil program. The main objectives here are to:

1. Prove out the concept of sealing off the exit vent after filling. Epoxy will work itself into all voids under atmospheric pressure on the supply side.
2. Study the effect of fill rate on impregnation quality and get further experience with the external resin trap in the vent side of the mold.
3. Study the effect of internal manifolding (resin passageways) on impregnation quality.
4. If time permits, look into applying positive pressure to the supply side of the fixture.

We will validate the process using the following tests and criteria:

Tests:

1. We will perform visual inspections of all surfaces.
2. After inspection of surfaces, we will section the test coils to inspect for full impregnation between windings.

Criteria:

1. No visible dry spots (places where wetting did not occur) anywhere on the fiberglass.
2. No epoxy voids greater than .02 in. between windings or greater than .06 in. on the surface of the coil.

It should be noted that the above tests and inspections will be repeated on the 4M copper coil when it is fabricated. The visual inspections will be conducted on all coils.

5. MECHANICAL DESIGN

a. General concept

The cross-section of the subscale magnet is shown in Fig. 5.1: the outer diameter is 304.8 mm and the longitudinal length is 3.6 m. A double-layer coil module is wound around a single iron pole (island) in a flat racetrack configuration and vacuum-impregnated with epoxy resin. Two of these modules are assembled in a common-coil configuration, and compressed on both sides by iron pads.

The proposed support structure comprises several components: pads, loading keys, yokes, and shell. Before the final assembly takes place, the components are assembled into two subassemblies. The first subassembly is composed of the two coils held together by two bolted iron pads. The pads provide initial pre-stress and alignment. The second subassembly is comprised of a 2-piece iron yoke and an outer aluminum shell. A gap is present between pad and yoke. The gap provides room for inserting pressurized bladders and is finally bridged by four interference keys.

Once the structure is locked by the keys, the bladders are deflated and removed. During cool-down, the shell generates additional pre-load on the coil-pack, as a result of the different thermal contractions of aluminum and iron.

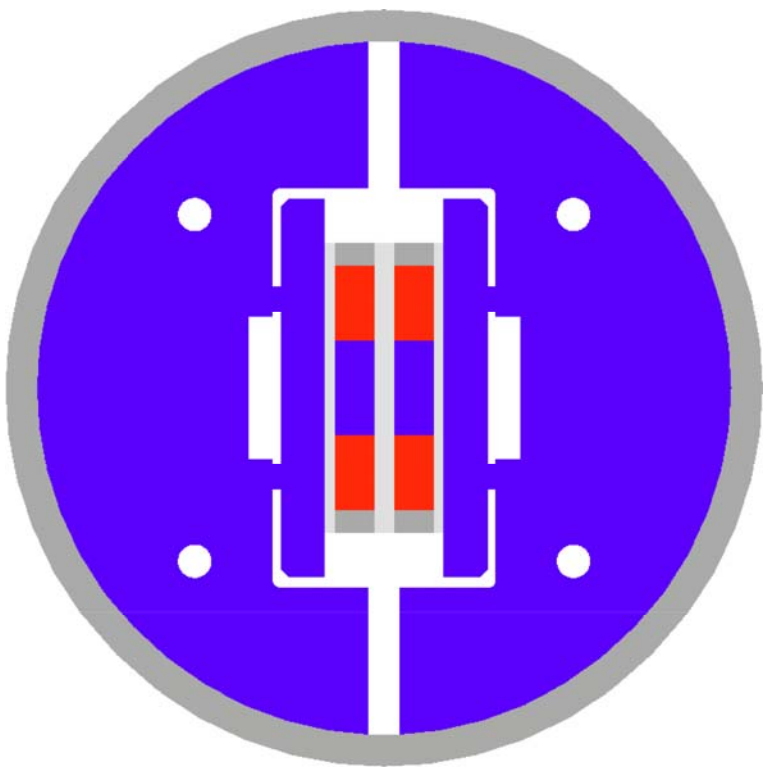

Fig. 5.1: Magnet cross-section.

With respect to the SM cross-section (Fig. 5.2)

- the shell ID has been increased to 305 mm (same shell thickness);
- the yoke halves are thicker with a larger gap;
- the pads have been simplified;

- the stainless steel skin thickness has been increased;
- slots have been included in the yoke design to facilitated bladder removal with thicker pull shims.

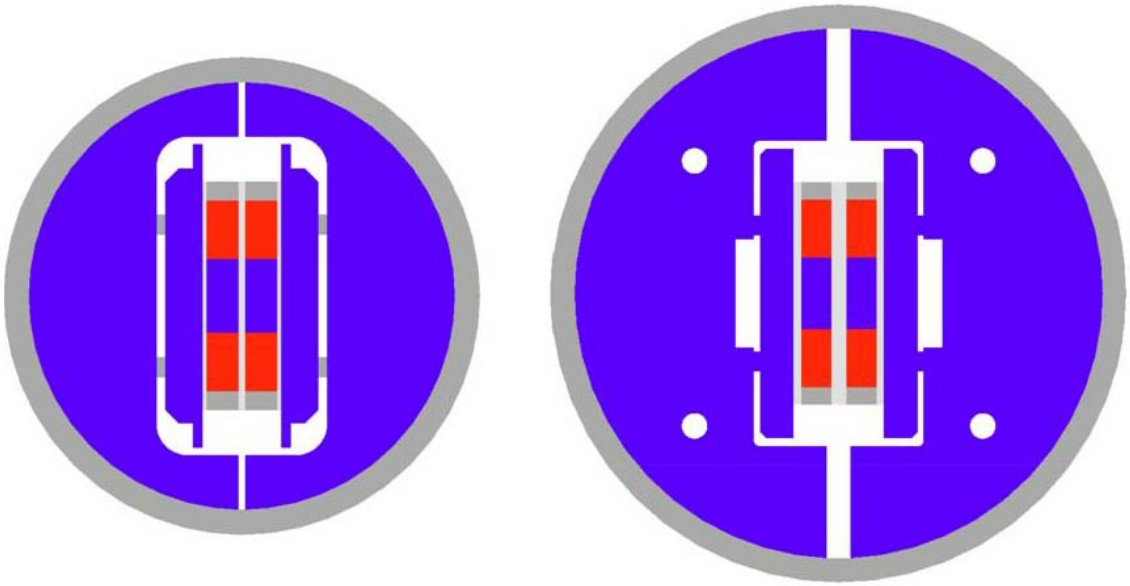

Fig. 5.2: Comparison between SM (left) and LR (right) cross-section.

b. 2D mechanical analysis and tolerance analysis

A 2D mechanical analysis of the cross section was performed aiming at finding the optimal pre-stress at room temperature and acceptable range. Tolerances were set in order to be always in the acceptable range even without taking into account the smoothing effect of the pads. Results are shown in Figures 5.3 to 5.6. The target pre-stress at room temperature is 60 MPa (190 MPa at 4.2 K).

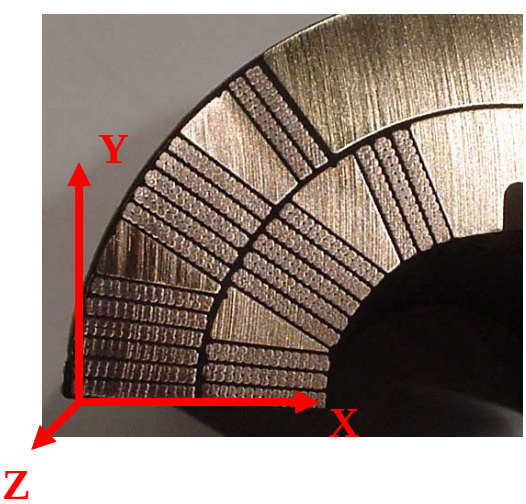

Material properties for FEM analysis

Parameter	**unit**		
Straight section		*293 K*	*4.3 K*
Ex – Radial direction	GPa	40	40
Ey – Azimuthal dir.	GPa	40	40
Ez – Longitudinal dir.	GPa	50	50
αx – Radial dir.	E-3	3.3	
αy – Azimuthal dir.	E-3	3.3	
αz – Longitudinal dir.	E-3	2.7	
Ends		*293 K*	*4.3 K*
Ex – Radial dir.	GPa	40	40
Ey – Azimuthal dir.	GPa	40	40
Ez – Longitudinal dir.	GPa	40	40
αx – Radial dir.	E-3	3.3	
αy – Azimuthal dir.	E-3	3.3	
αz – Longitudinal dir.	E-3	3.3	

Legend: E is the elastic module, α is the integrated thermal contraction from 293 K to 4.3 K

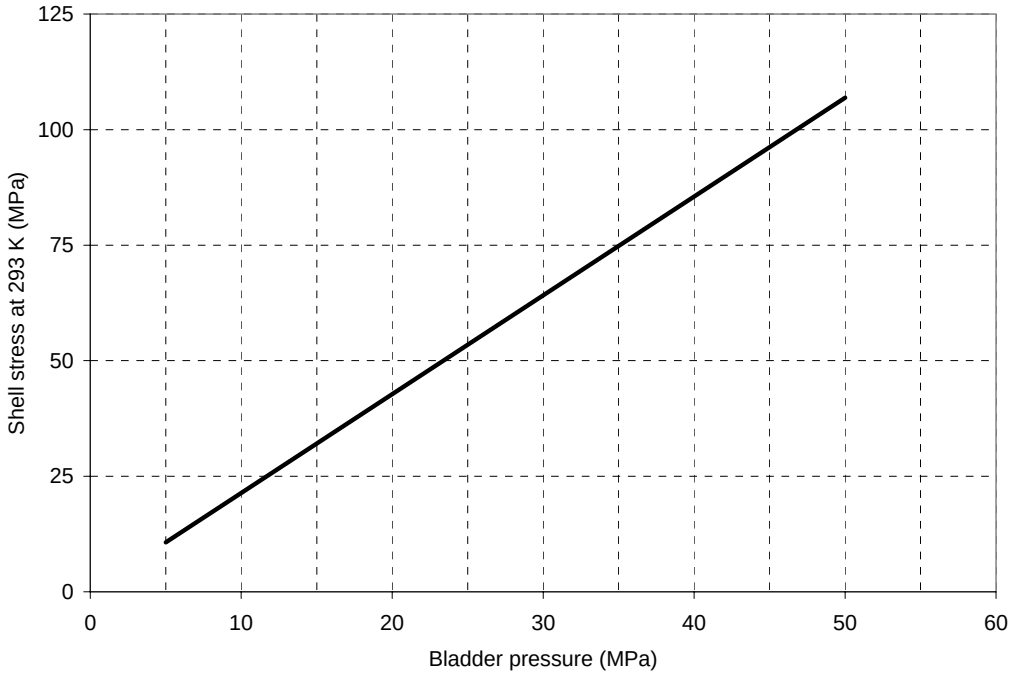

Fig. 5.3: Shell stress at 293 K (MPa) as a function of bladder pressure (MPa).

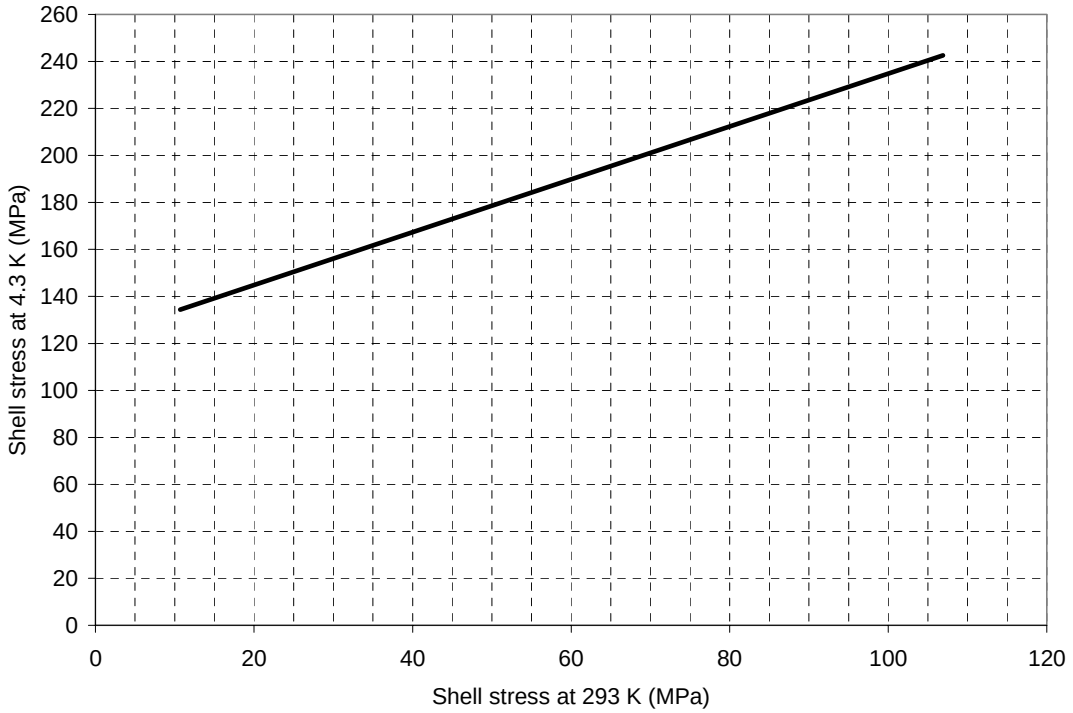

Fig. 5.4: Shell stress at 4.3 K (MPa) as a function of shell stress at 293 K (MPa).

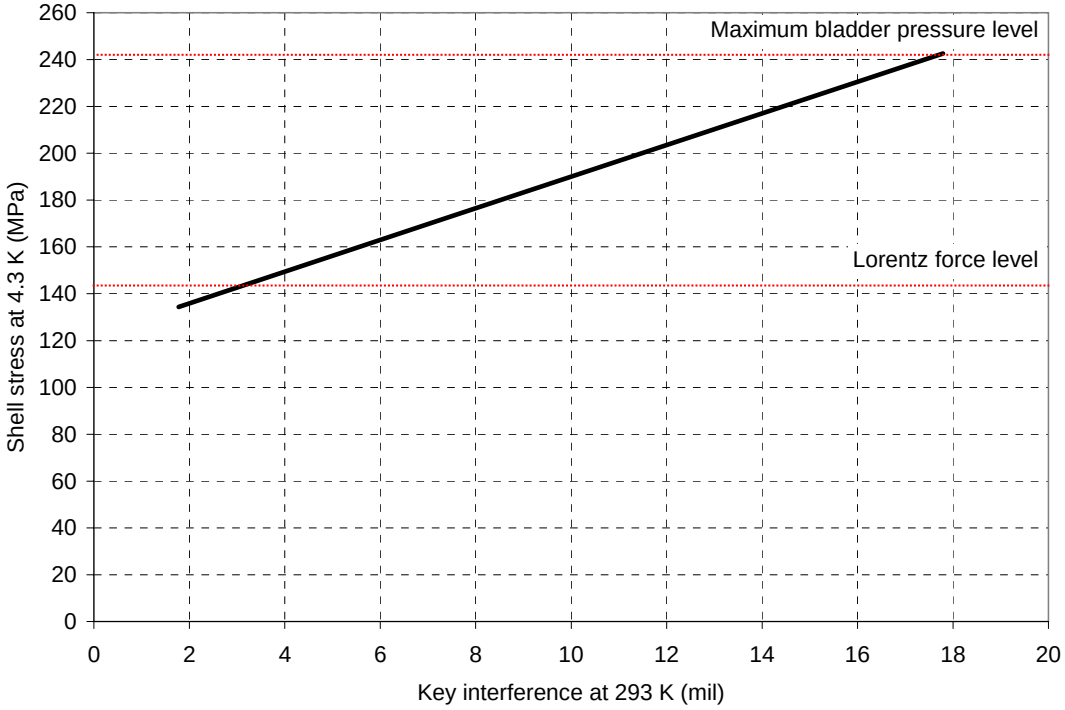

Fig. 5.5: Shell stress at 4.3 K (MPa) as a function of key interference (mil).

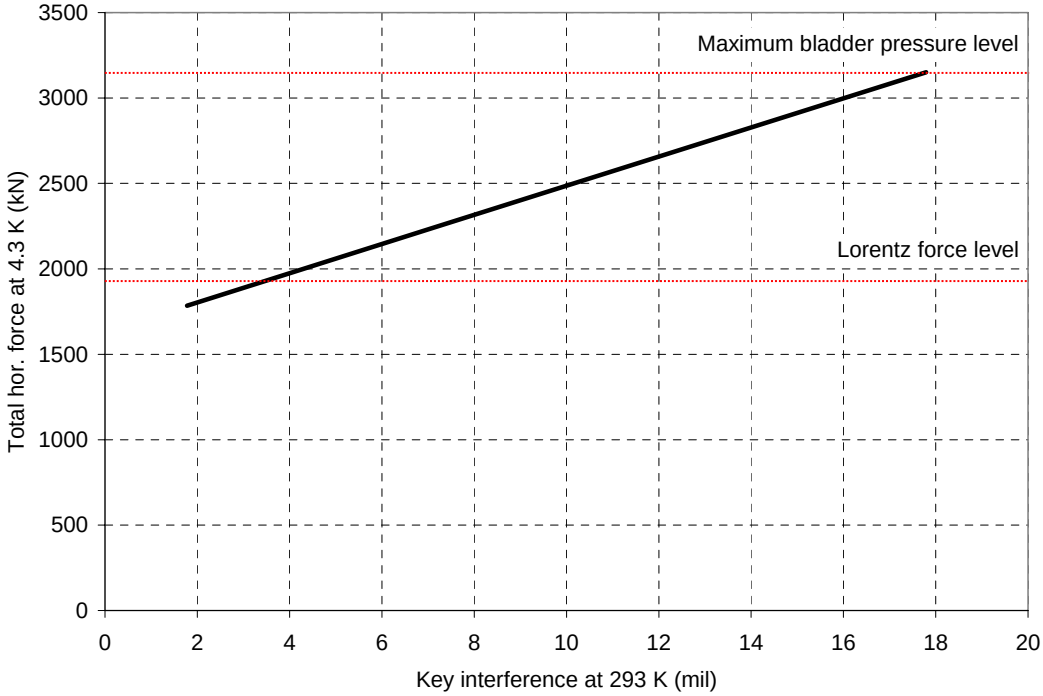

Fig. 5.6: Total horizontal force provided by the shell to the coil pack at 4.3 K (MPa) as a function of key interference at 293 K (mil).

Tolerance for cross-section parts

	Inch	mm
Shell ID:	0.000 / + 0.0025	0.000 / + 0.064
Yoke OD:	0.003 / + 0.000	0.076 / + 0.000
Yoke key slot:	0.002 / + 0.002	0.051 / + 0.051
Pad thickness:	0.003 / + 0.003	0.076 / + 0.076
Total range:	**0.008 / + 0.008**	**0.200 / + 0.200**

The Lorentz forces tend to separate the coil modules (Fig. 5.7, left). To limit the coil motion during excitation, the shell is pre-tensioned at room temperature to the nominal stress of 45 MPa. After the cool-down, the shell tension increases up to 175 MPa, and the corresponding force transmitted to the coil is of about 2.2 kN/mm. Due to the different thermal contraction between the coil module components, after cool-down the force produced by the shell is mainly transmitted to the iron island and the stainless steel rails, which feature a lower thermal contraction than the coil (Fig 5.7, right).

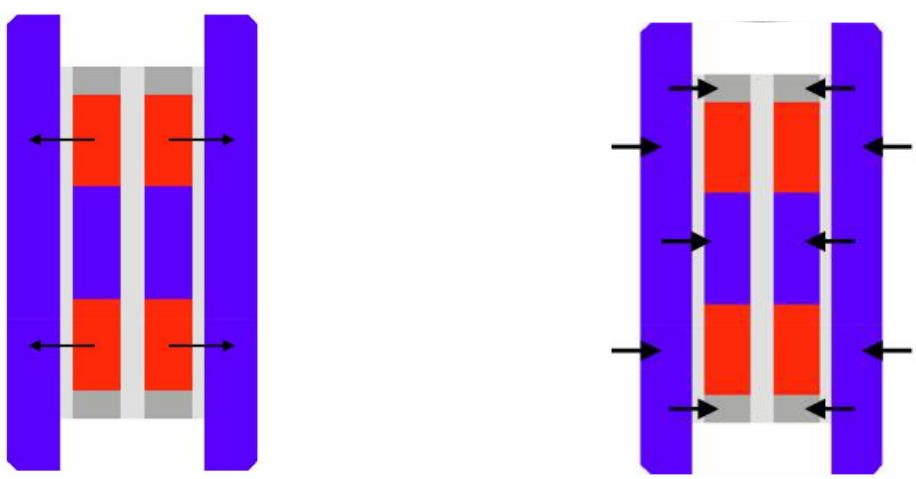

Fig. 5.7: Lorentz force (left) and pre-stressing force (right) directions.

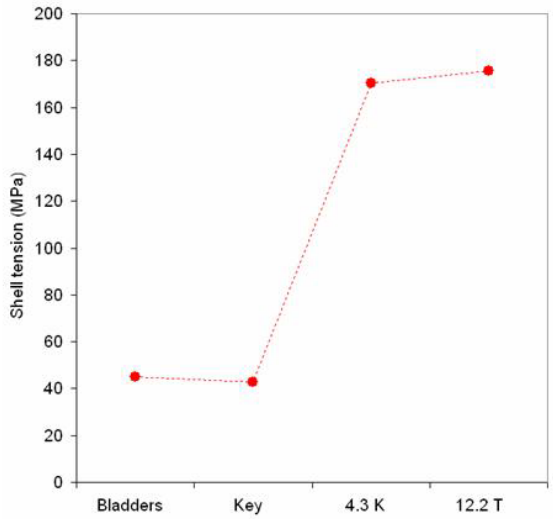

Fig. 5.8: Shell tension during assembly, cool-down, and excitation.

The coil is therefore characterized by a low horizontal stress after cool-down (30 MPa, Fig. 5.9 left), and by a higher stress of 75 MPa at short sample current (Fig. 5.9, right). During all magnet operations, the yoke tension is kept below 100 MPa (Fig. 5.10).

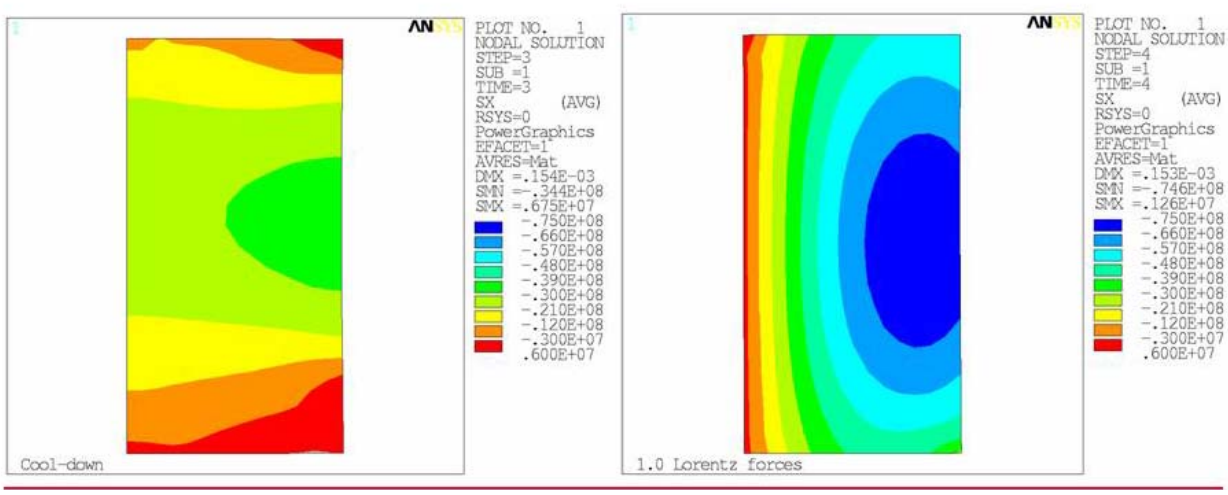

Fig. 5.9: Coil horizontal stress (Pa) after cool-down (left), and at short sample current (right).

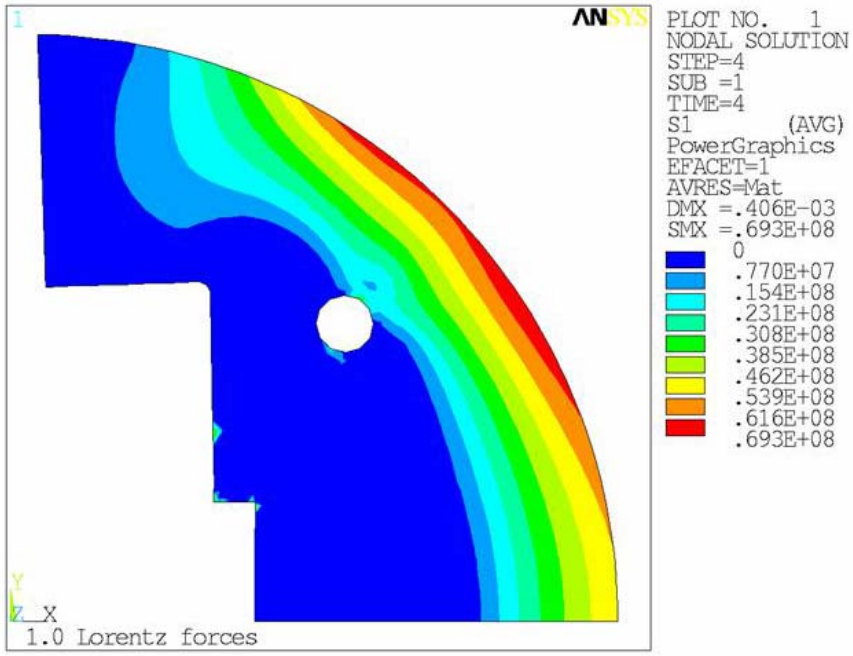

Fig. 5.10: Yoke tension (Pa) at short sample current.

c. 3D mechanical analysis

In Fig. 5.11 we show the 3D mechanical model. To reduce the CPU time, we reduced the total length of the coil straight section to about 300 mm (twice as long as the current short subscale coils). We focused the analysis on the mechanical behavior of the coil (Fig. 5.12, left) with respect to the supporting structure, pointing out the effect of Lorentz force on the contact region between the innermost turn and the iron island (Fig. 5.12, right). Two cases have been considered:

1. Frictionless model, with coil allowed separating from the island (Fig. 5.13-14)
   - The contact force between the coil and the island after cool-down is F_z = 17 kN per quadrant
   - In average, the coil features a tension in the z direction of 18 MPa, and the island a compression in the z direction of 55 MPa
   - In the straight section, the coil is separating from the island.
2. Friction model (μ=0.2), with coil allowed separating from the island (Fig. 5.15-16)
   - The contact force between the coil and the island after cool-down is F_z = 11 kN.

The interaction between shell and yoke has been analyzed with a full-length 3D model (Fig. 5.17). The relative displacement between shell and yoke at 4.3 K has been considered, assuming a shell stress of 150 MPa at 4.3 K.

- Frictionless model (Fig. 5.18)
  a. Shell axial contraction = 9.5 mm
     i. 9.5 mm = (4.2e-3 * 2000 + 150 / 79000 * 0.3 * 2000) mm = 8.4 + 1.1 mm
  b. Yoke axial contraction = 3.9 mm
     i. 3.9 mm = (1.97e-3 * 2000) mm
  c. Relative displacement shell-yoke = 5.6 mm
- Friction model (μ = 0.2) (Fig. 5.19)

a. Shell axial contraction = 5.7 mm
b. Yoke axial contraction = 4.2 mm
c. Relative displacement shell-yoke = 1.5 mm

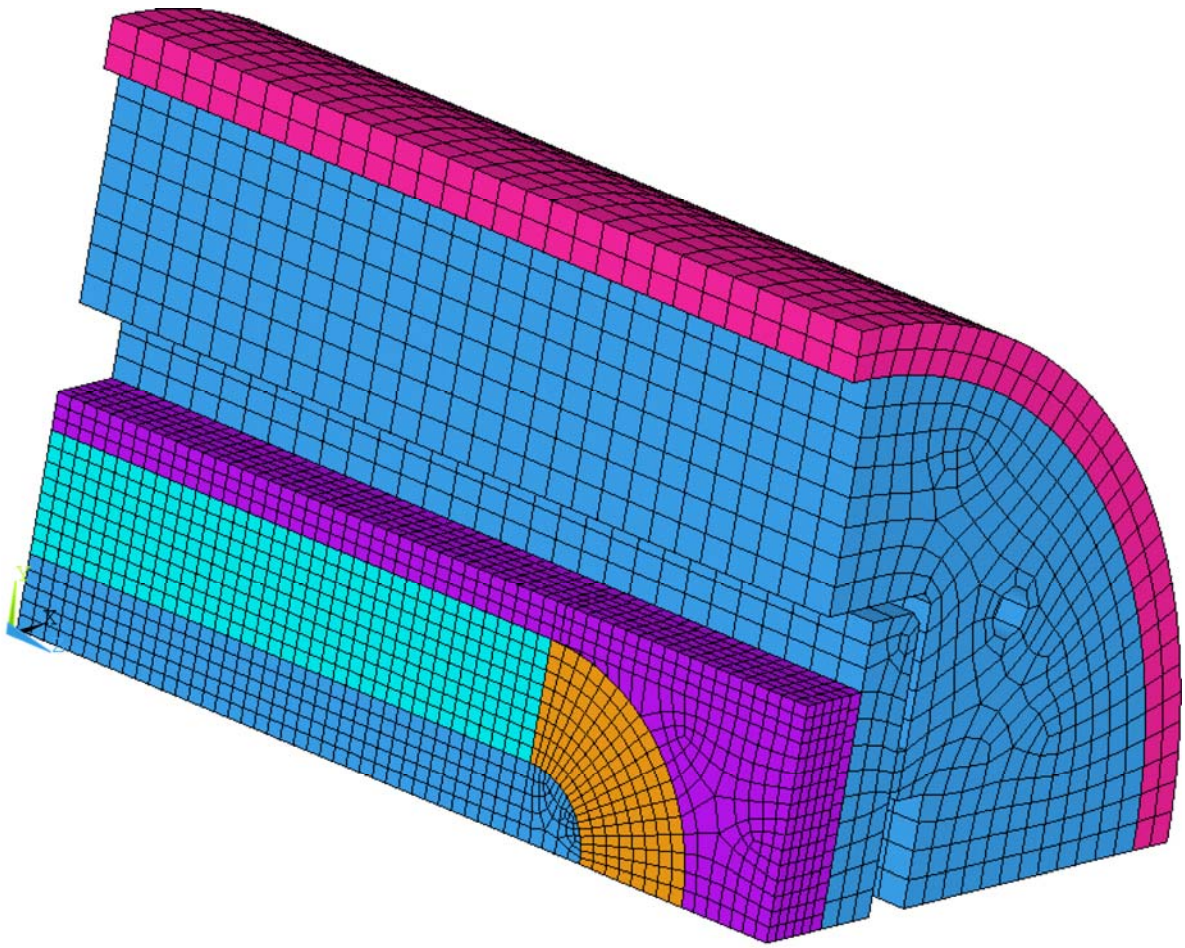

Fig. 5.11: 3D finite element model of the entire geometry.

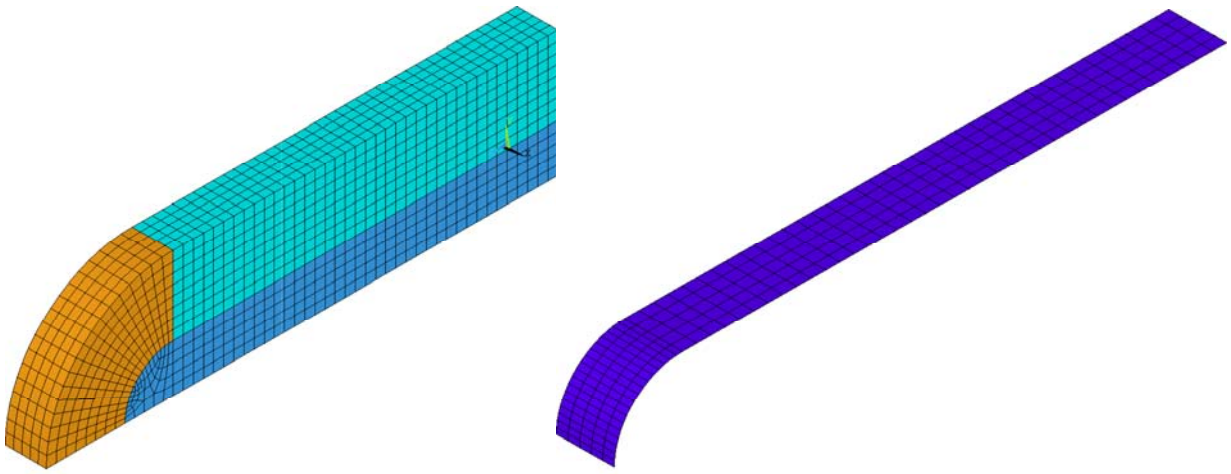

Fig. 5.12: 3D finite element model of the coil and contact elements between coil and island.

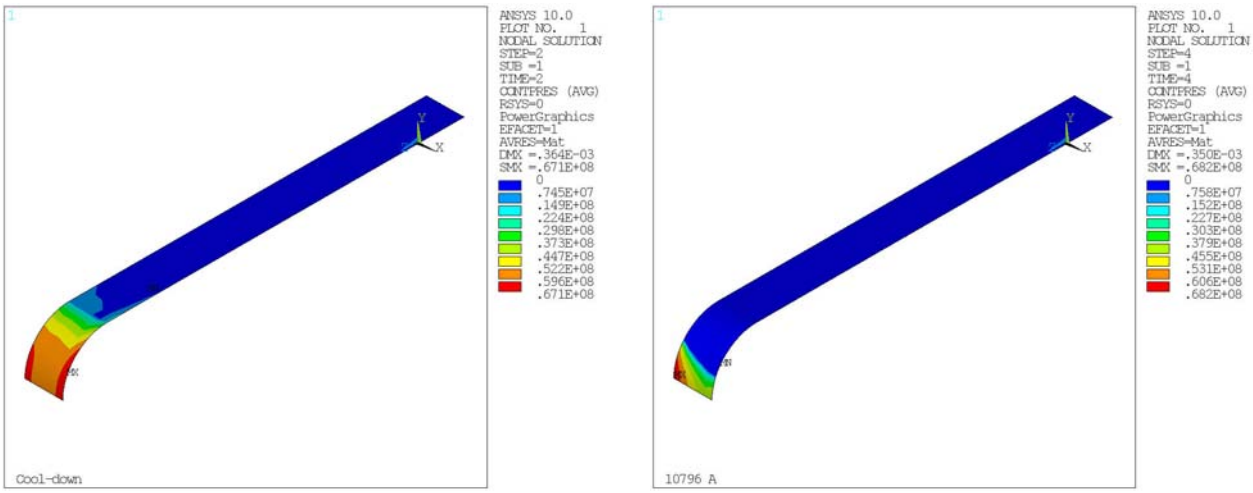

Fig. 5.13: Frictionless model, with coil allowed separating from the island: contact pressure between coil and island after cool-down and at short sample (10.80 kA).

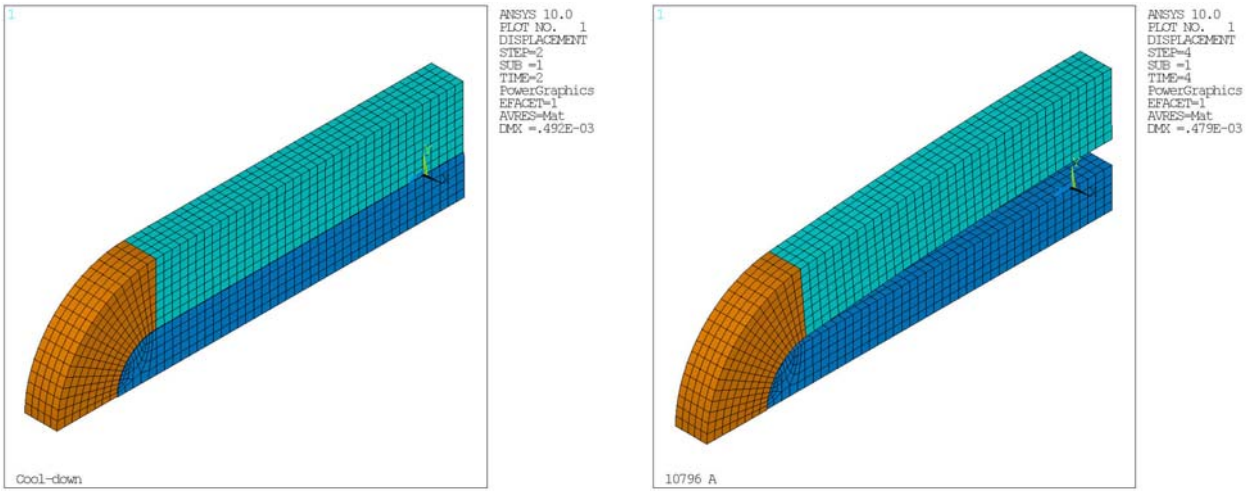

Fig. 5.14: Frictionless model, with coil allowed separating from the island: deformed shape (displacement scaling: 20) after cool-down and at short sample (10.80 kA).

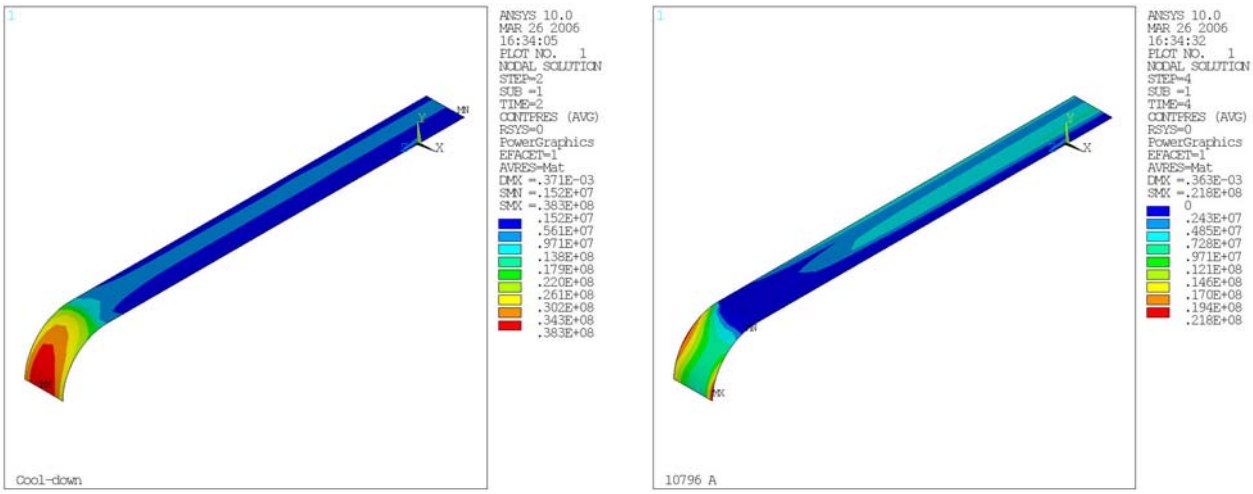

Fig. 5.15: Friction model (μ=0.2), with coil allowed separating from the island: contact pressure between coil and island after cool-down and at short sample (10.80 kA).

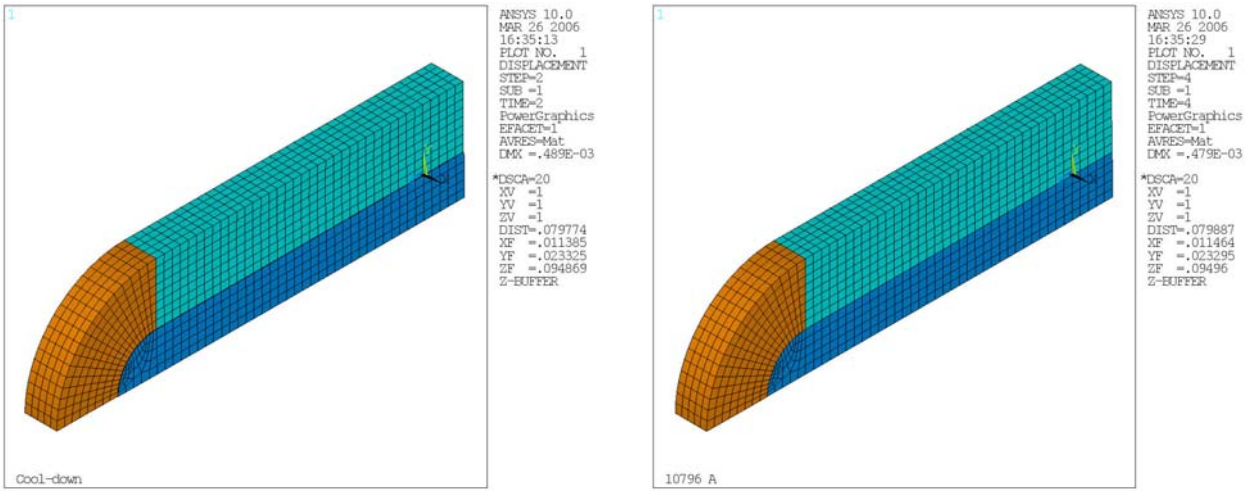

Fig. 5.16: Friction model (μ=0.2), with coil allowed separating from the island: deformed shape (displacement scaling: 20) after cool-down and at short sample (10.80 kA).

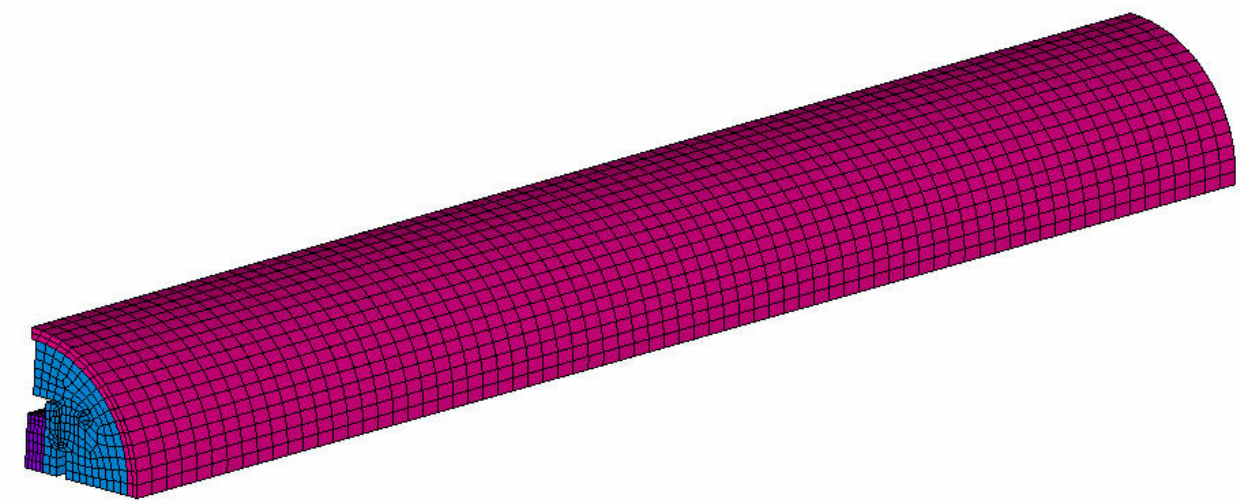

Fig. 5.17: Full length mechanical model.

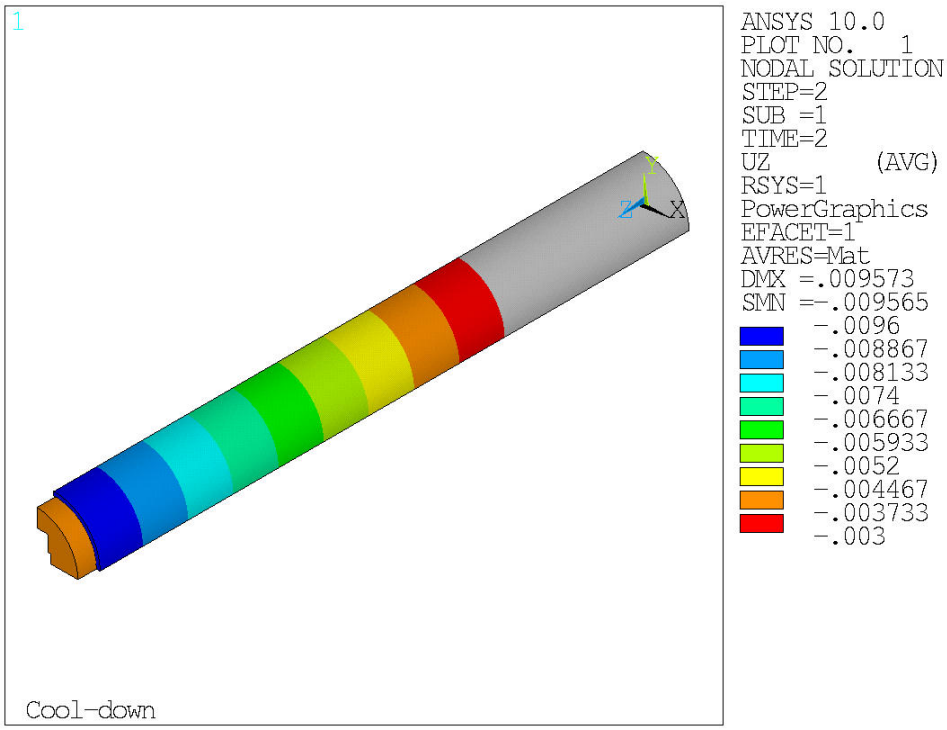

Fig. 5.18: Axial displacement of shell and yoke at 4.3 K (frictionless model).

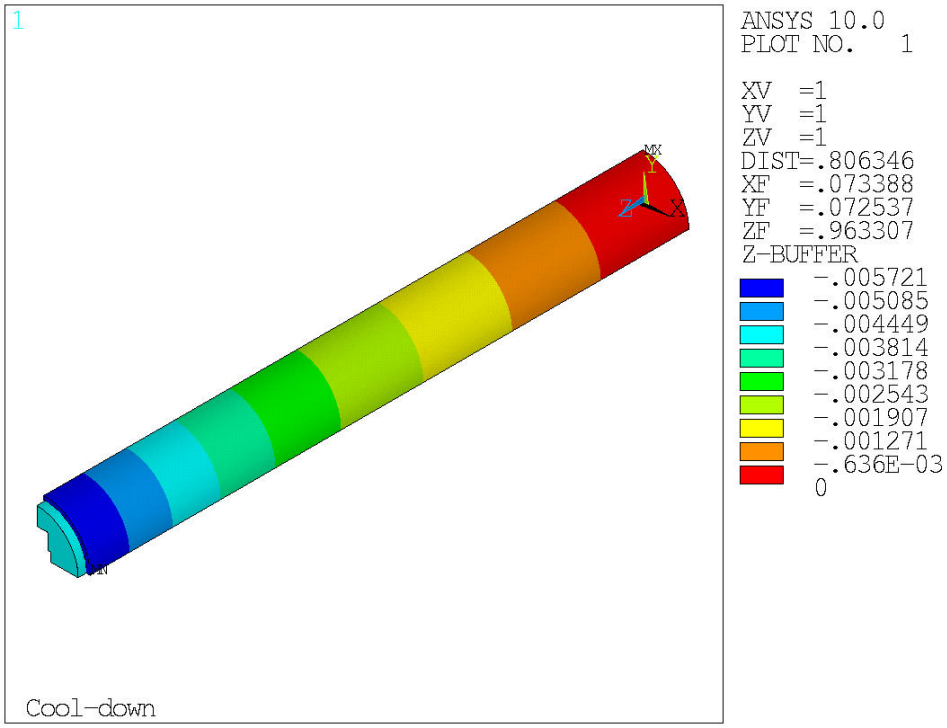

Fig. 5.19: Axial displacement of shell and yoke at 4.3 K (friction model).

d. Test of the supporting structure

i. Assembly and handling

We provide below a detailed description of the assembly steps, which are shown in Fig. 5.20 – 25.

1 Initial Setup
1.1 Setup 24' of granite table
1.2 Place lower raft onto table - use jacking screws in lifting-eye bolt holes in bottom of raft
1.3 Place LR Al shell onto lower raft

2 Installation Raft Configuration
2.1 Mount installation beam onto upper raft with “tall" standoffs - "Tall Standoffs" place the inserted yokes approx. 250" from theoretical center (may be less)
2.2 Mount cantilever beam cradle supports - The cradles support the beam while inside the Al tube.
2.3 Attach cantilever/carrier beam to installation raft
2.4 Mount sacrificial brass keys on pad key slots of the installation beam
2.5 Insert cantilever/carrier beam into empty Al shell, align

3 Insertion of first yoke half into shell
3.1 Align and pin rest of 71 laminations - May have to insert threaded rods before (maybe not)
3.2 Tie with nuts on the 1/2" rods - What's the torque/clamping force necessary?
3.3 Apply moly lube to radial of yoke half assembly
3.4 Slide first yoke half into shell - brass keys will slide on cantilever beam slots (not the laminations)
3.5 Disconnect cantilever beam from installation raft
3.6 Move installation raft out of the way
3.7 Insert (dummy?) pull shims into yoke bladder slot
3.8 Attach High Pressure pump to manifold at the opposite end of cantilever beam - Manifold connects to five Enerpac RC-50 cylinders inside cantilever/carrier beam, each with .625" stroke
3.9 Pressurize cylinders to ~270-300 psi - Assumes 1350 lbs. distributed by 5 sq. in (each RC-50 cylinder has 1 sq in. effective area)
3.10 Valve out HP pump from manifold - Manifold and cylinders remain at 300 psi
3.11 Disconnect HP pump

4 Assembly Rotation
4.1 Remove installation beam and "tall" standoffs from installation raft
4.2 Mount the upper raft to the top of magnet structure, secure bolts
4.3 Mount Aluminum discs to the raft ends
- Bolt yoke half to discs via tie-rods
- Bolt raft to discs

4.4 Lift assembly onto floor
4.5 Roll assembly 180 degrees - Brass sacrificial keys may rattle around, as they're no longer constrained. Remove beforehand?
4.6 Lift assembly back onto granite table
4.7 Remove Aluminum discs from ends
4.8 Release pressure in cylinder manifold - Does this require reconnecting the HP pump?

5 Installation Raft reconfiguration
5.1 Unbolt upper raft from shell assembly
5.2 Lift upper raft, flip, and set down
5.3 Mount installation beam on "tall" standoffs
5.4 Bring installation raft to the end of the shell assembly
5.5 Re-attach cantilever beam to installation raft
5.6 Extract cantilever beam and set raft on table - Do not remove the pull shims or sacrificial keys from installed yoke (if still installed. After this operation would be a good time to re-insert keys, if they were removed.)--they'll be used for the second yoke half installation.

5.7 Remove the cradle supports from the cantilever/carrier beam.
5.8 Re-insert cantilever beam into Al shell assembly - The cantilever beam should now be resting on the sacrificial keys, and the cylinders will be facing upside down, toward the pull shim.

6 Insertion of second yoke half into shell
6.1 Align and pin 71 laminations - May have to insert tie rods before laminations
6.2 Tie with the 1/2" rods - What's the torque value?
6.3 Apply moly lube to radial of yoke half assembly
6.4 Slide yoke half into shell - brass keys will slide on cantilever beam key slots
6.5 Disconnect cantilever beam from installation raft and move raft out of the way
6.6 Connect HP pump to cylinder manifold in cantilever beam
6.7 Pressurize to 270-300 psi - the cylinders are acting downward
6.8 Insert gap keys to separate yoke halves - According to calculations, a continuous four-span supported beam will deflect max <.002", so maybe use ~.490" gap keys?
6.9 Release pressure in manifold - Yoke halves will now be resting on gap keys, not the brass sliders
6.10 Disconnect HP pump from manifold

7 Installation raft -> Coil installation re-configuration
7.1 Re-attach installation raft to carrier/cantilever beam
7.2 Extract the cantilever beam, and place installation raft assembly on table
7.3 Disconnect cantilever beam from installation raft
7.4 Remove installation beam
7.5 Replace "tall" standoffs with "short" standoffs - these standoffs set the 3x5 beam slots at the same level as the bottom yoke key slots
7.6 Re-attach installation beam

8 Coil Stack Installation
8.1 Assemble coil stack* (load pads, dummy coil, skins, etc.)
8.2 Align installation raft to Al shell assembly
8.3 Lay lubed, full-height, steel keys in installation raft slots
8.4 Lift coil stack onto keys on installation raft keys
8.5 Insert coil stack - Stack will slide with the steel keys
8.6 Insert bladders into the upper bladder yoke slot w/pull shims
8.7 Pressurize and insert load keys - with Fuji paper?
8.8 Remove gap keys
8.9 Un-pressurize

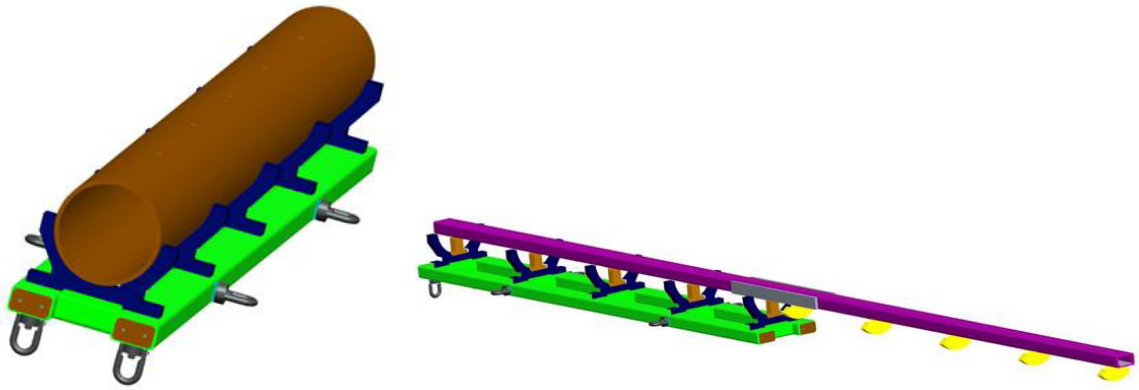

Fig. 5.20: Shell on the raft and assembly beam.

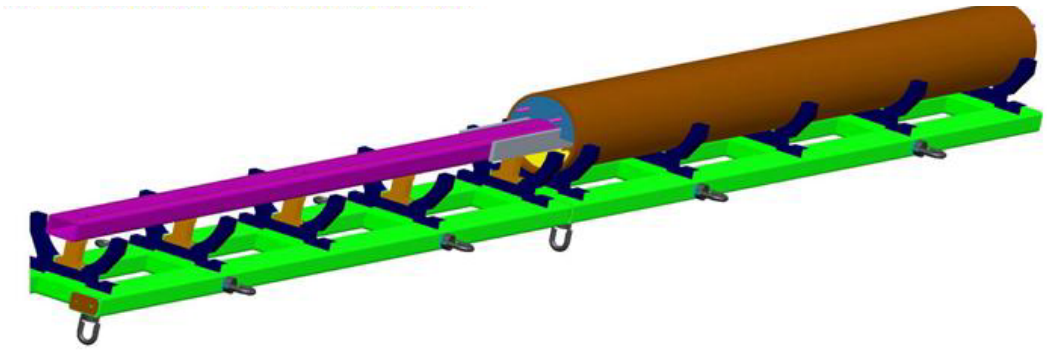

Fig. 5.21: Insertion of first yoke half.

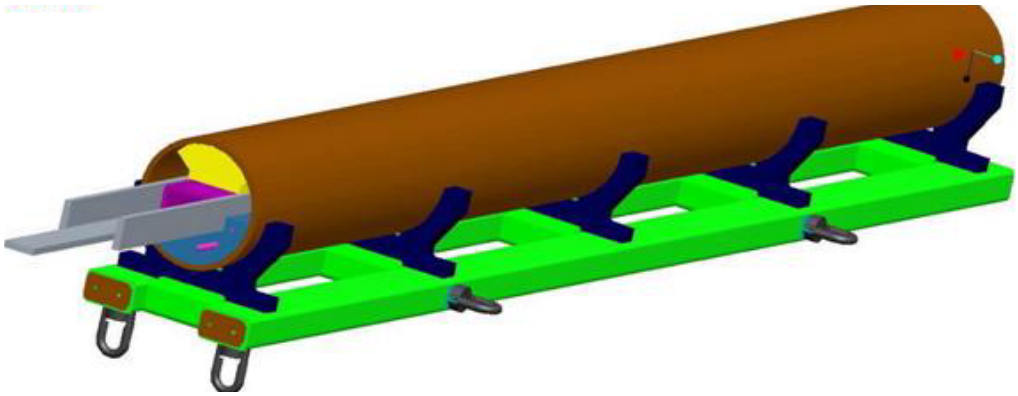

Fig. 5.22: Rotation of the structure.

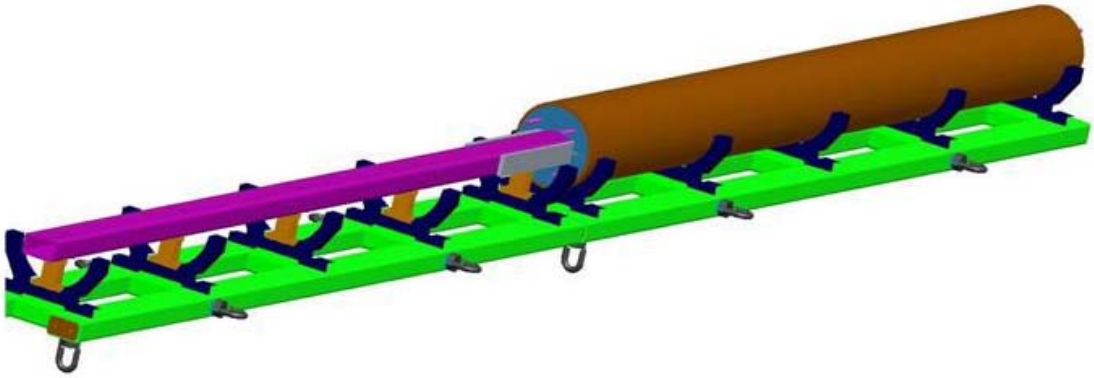

Fig. 5.23: Insertion of second yoke half.

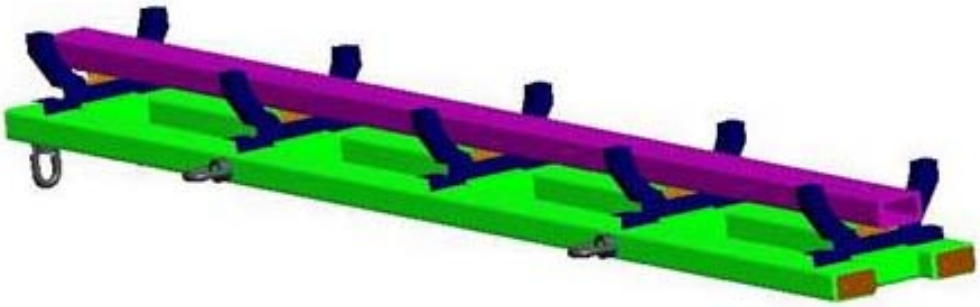

Fig. 5.24: Reconfiguring of raft/beam.

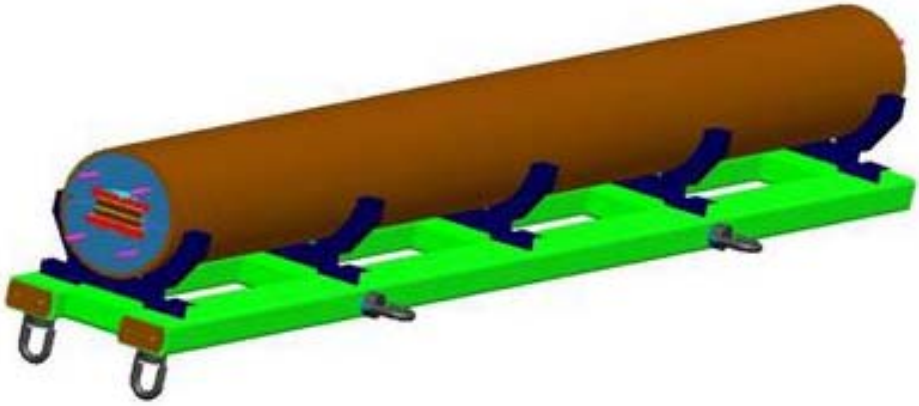

Fig. 5.25: Insertion of coil pack.

ii. Instrumentation

The goal of the instrumentation on the supporting structure is to monitor stresses in the supporting structure during assembly, cool-down, and energization, and compare with FEM predictions.

Twenty strain gauges will be used, each one with a dedicated compensator gauge. They will be located at 5 longitudinal locations, on two sides, two per side (in order to measure both in longitudinal and azimuthal direction).

iii. Test plan

Once the magnet is fully assembled and instrumented, the test plan will include:

- Pressurization of bladders and key insertion in several steps (approximately 500 PSI bladder pressure step).
- Measurement of shell stress level and uniformity with strain gauges.
- Disassembly and inspection of pressure sensitive films.

6. MAGNET ASSEMBLY

The magnet assembly procedure will be finalized after testing the supporting structure and practice with magnet assembly using dummy coils.

7. QUENCH PROTECTION

a. Quench Propagation Calculations

In order to design an adequate quench protection system for the LRS01 racetrack magnet, calculations were performed by using the code QUENCHS, a quench propagation program based on an earlier program developed by Martin Wilson and his colleagues at Rutherford Laboratory in Great Britain [7.1, 7.2]. This program assumes a rectangular, Cartesian geometry model representative of real magnet coils, and makes use of the conductor, cable, and coil parameters. The program also takes into consideration the specific heats and thermal conductivities of the various materials that make up the conductor, in this case Nb_3Sn, copper, and insulator. It is therefore not an adiabatic model, since it does include the effect of heat transport to the insulation. Though this program does have the capability of calculating quench propagation velocities, it was decided to assume the value of the quench velocity as an input, as this would most likely give the best estimates of quench maximum temperature, internal coil voltage, and the value of the integral $\int I^2 dt$ in miits, over a range of possible quench velocities. Two positions were assumed for the quench origin, one at the edge of the coil block and one in the interior of the coil.

The results of the calculations for quench velocities of 1, 10, 50, and 100 m/s and for the interior and the edge are given in the Tables 1-8. The slow 1 m/s quench velocity is somewhat unrealistic but is included for completeness.

Table 1 1 m/s interior

CURRENT (A)	TEMP (K)	Int(I**2dt) miits	VOLTAGE volts
2000	170.88	3.45	14.1
3000	426.45	6.01	28.7
4000	950.16	8.71	48.6
5000	1788.45	11.44	75.0
6000	2877.96	14.22	106.4
7000	4128.35	17.09	140.9
8000	5480.72	20.09	176.8
9000	6893.46	23.24	213.5
10000	8354.40	26.55	250.5

Table 2 10 m/s interior

CURRENT (A)	TEMP (K)	Int(I**2dt) miits	VOLTAGE volts
2000	62.57	1.27	25.6
3000	105.74	2.32	55.5
4000	164.87	3.35	102.1
5000	249.51	4.45	156.8
6000	372.01	5.61	222.5
7000	544.62	6.84	302.6
8000	779.23	8.09	397.5
9000	1078.21	9.36	507.1
10000	1445.39	10.61	630.3

Table 3	50 m/s	interior	
CURRENT (A)	TEMP (K)	Int(I**2dt) miits	VOLTAGE volts
2000	43.11	0.64	46.0
3000	61.91	1.25	84.7
4000	86.40	1.91	143.7
5000	117.51	2.55	233.2
6000	153.31	3.19	334.6
7000	196.83	3.88	446.0
8000	251.34	4.58	573.4
9000	318.45	5.29	720.8
10000	398.91	5.98	888.2

Table 4	100 m/s	interior	
CURRENT (A)	TEMP (K)	Int(I**2dt) miits	VOLTAGE volts
2000	38.18	0.47	61.2
3000	52.39	0.95	107.6
4000	69.66	1.48	172.9
5000	91.08	2.02	266.3
6000	116.25	2.54	397.4
7000	144.23	3.09	536.0
8000	177.94	3.66	687.2
9000	216.81	4.22	855.2
10000	264.12	4.77	1042.2

Table 5	1 m/s	edge	
CURRENT (A)	TEMP (K)	Int(I**2dt) miits	VOLTAGE volts
2000	214.23	4.04	12.3
3000	582.93	7.00	24.9
4000	1326.99	10.06	43.1
5000	2441.25	13.15	66.5
6000	3802.30	16.33	93.3
7000	5305.81	19.67	122.0
8000	6898.93	23.21	151.3
9000	8546.48	26.97	181.0
10000	10240.19	30.96	210.9

Table 6	10 m/s	edge	
CURRENT (A)	TEMP (K)	Int(I**2dt) miits	VOLTAGE volts
2000	64.91	1.35	26.2
3000	114.74	2.50	56.6
4000	188.56	3.70	100.8
5000	302.13	4.98	152.8
6000	474.20	6.35	214.4
7000	722.43	7.78	287.2
8000	1058.81	9.24	370.9
9000	1478.28	10.69	465.4
10000	1976.25	12.13	569.4

Table 7	50 m/s	edge	
CURRENT (A)	TEMP (K)	Int(I**2dt) miits	VOLTAGE volts
2000	43.28	0.64	46.4
3000	62.51	1.27	85.5
4000	88.18	1.95	144.9
5000	121.67	2.62	234.1
6000	161.14	3.31	341.2
7000	210.34	4.05	457.7
8000	273.79	4.82	587.2
9000	354.17	5.60	736.6
10000	453.48	6.37	905.3

Table 8	100 m/s	edge	
CURRENT (A)	TEMP (K)	Int(I**2dt) miits	VOLTAGE volts
2000	38.22	0.48	61.5
3000	52.53	0.95	108.2
4000	70.07	1.49	173.8
5000	92.21	2.04	267.7
6000	118.43	2.59	397.8
7000	148.24	3.15	546.5
8000	184.01	3.74	698.6
9000	226.58	4.34	870.9
10000	278.32	4.92	1062.5

As can be seen, quench temperatures and internal coil voltages can get high enough under some circumstances to cause coil performance degradation and possibly even fatal damage to the conductor or insulation. For example, it has been shown that quenches above 400K can result in degradation of performance due to thermo-mechanical stresses [7.3]. It would therefore be prudent to keep quench

temperatures below 300K. Also, internal voltages approaching 1000V may result in insulation failure, so such voltages should be kept below a safe value.

It can also seen that quench temperatures are higher for edge quenches than for interior quenches, as expected. Figure 7.1 shows temperature variation with quench current for 10 m/s and 50 m/s for both edge and interior quenches.

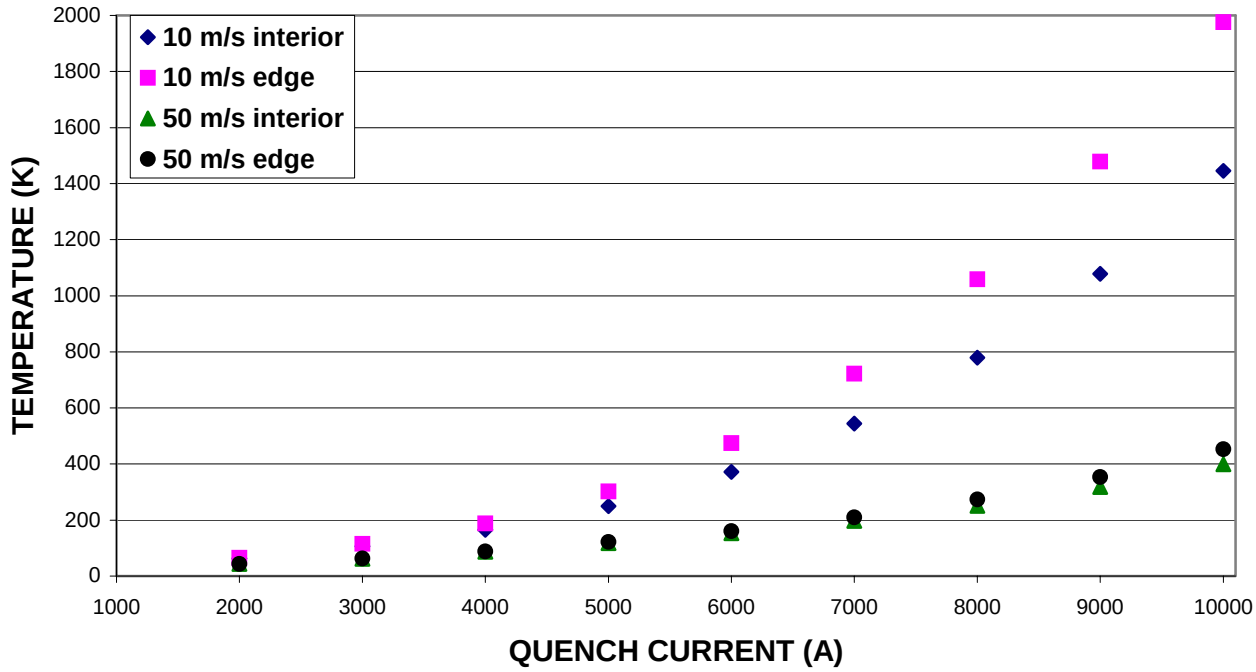

Fig 7.1. Quench temperature variation with quench current for edge and interior locations.

In Figure 7.2 the calculated values of $\int I^2 dt$ in miits vs. maximum quench temperature are plotted for all quench velocity cases. The miits-temperature behavior is independent of quench velocity. This shows that in order to keep the quench temperature below 300K, miits must be limited to less than 5. This has already been shown to be a safe limit in the case of SQ01 testing at Fermilab [7.4]. SQ magnets have also used the 20-strand RRP cable. No actual temp-miits measurements for this type of cable have been done so far. Such tests using spot heaters and voltage taps are planned at BNL on a short sample of the actual 20-strand RRP cable prior to actual testing of the LRS01.

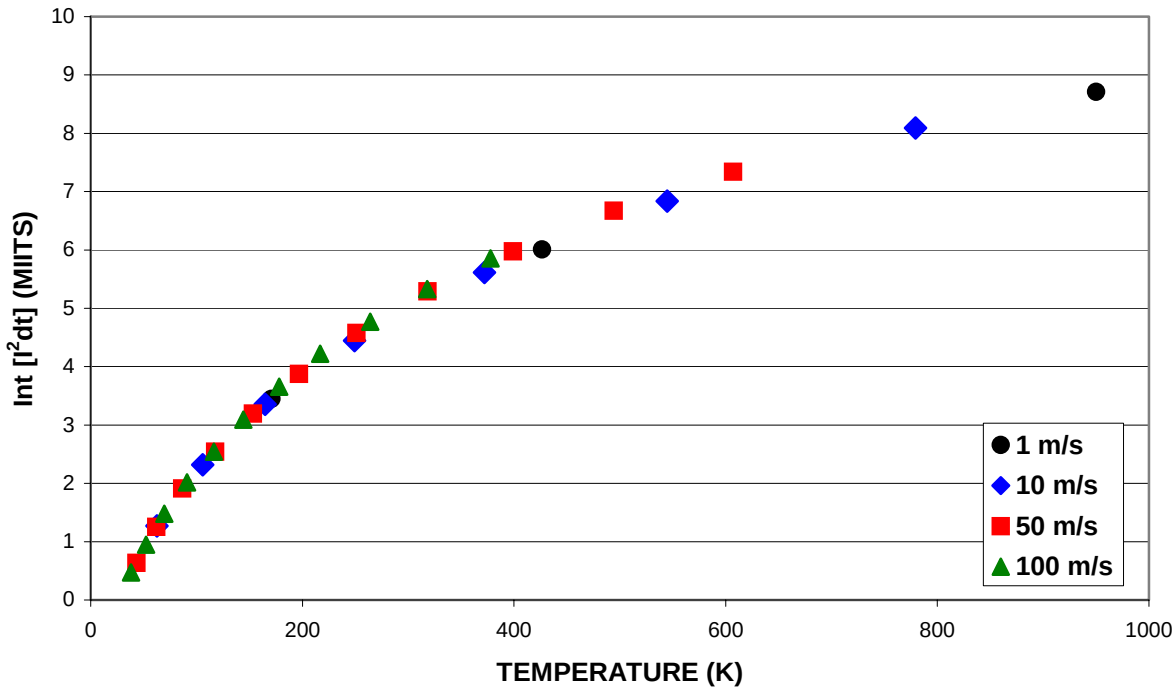

Fig 7.2. Calculated values of $\int I^2 dt$ and quench hot spot temperature for the RRP 54/61 20-strand cable.

The results of the calculations, as presented above, imply that quench protection of the LRS01 racetrack magnet will be required. This must be done in order to limit quench hot spot temperatures to 300K or less and to limit internal coil voltages to 500V or less. Such protection will be done using two methods: energy extraction to an external dump resistor, and a system of active quench protection heaters which will spread the stored energy into heat more uniformly over the entire coil.

b. Energy Extraction

First, an energy extraction system (quench protection assembly, or QPA) will be in place. A simplified representation of such a system is shown in Figure 7.3 and includes a switch in parallel with an external resistor. The actual assembly will include a combination of water-cooled IGBT switches in parallel and an air-cooled variable dump resistor bank. At this time, there are a sufficient number of switches in parallel to handle currents of up to15kA. (The expected quench current for the LRS01 is about 10kA.) The value of the variable dump resistance will be determined by the need to limit the total coil voltage to less than 500V.

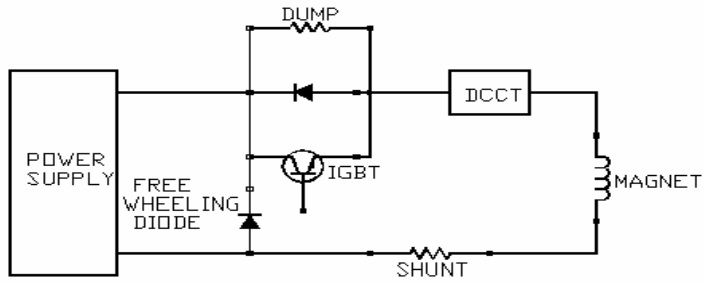

Fig 7.3. Simplified schematic of quench protection assembly to be used for energy extraction in LRS01.

c. Quench Protection Heaters

Quench protection heaters will also be used and are included on the LRS01 instrumentation trace, also called a flexible circuit, and will run along the inner and outer surfaces of both coils, with one strip covering half of both sides of each coil surface. Each surface of both coils will be covered by two of these half flexible circuits with a 0.82 m space in between where there is no instrumentation and no flexible circuit. Each half flexible circuit will contain one strip heater which loops around to cover both sides of its half of the coil surface. The strip heaters will be configured into two independent strip heater circuits, fired by capacitive discharge with two independent power supplies. This will insure that both the inner and outer surfaces of both coils will be quenched even if one circuit fails.

This quench protection heater system has been designed to provide maximum coverage over all turns on each straight section of each racetrack coil and also to provide redundancy in the event of the failure of one of the independent circuits. Each of the eight straight sections will be covered across all 21 turns by strips of type 304L austenitic stainless steel of thickness 0.0254 mm (0.001”) and width 3 cm or wider. At four locations along each strip, cutouts are introduced, where the strip width narrows down from to 1 cm, and these are spaced 0.72 m, 0.98 m, and 0.72 m apart along each coil straight section. This spacing can be shown to be adequate by assuming a realistically low quench propagation velocity of 10m/s. At this speed, for the widest spacing of 0.98 m, it would take each quench front 50 ms to meet at the halfway point between the cutout heaters and fill the entire 1 m section. In fact, it can be argued as well that the 1 m spacing is adequate even with a quench velocity of 5 m/s, since half of the 1 m section will be normal by 50 ms.

Each cutout consists of a section of width 1 cm and of varying length depending on what other instrumentation is present. The total resistance of each strip with the four cutouts is 3.1 Ω. The strips have been designed to accommodate other instrumentation such as voltage taps and spot heaters with which they will have to share space on the flexible circuit. Figure 7.4 shows a drawing of the flexible circuit design, including the strip heater cutout geometry and the locations of the various instrumentation devices. For simplicity in fabrication, all straight sections will have the same flexible circuit design scheme of heater geometry and tap/spot heater configuration. This has the added benefit of allowing more taps and spot heaters if wanted.

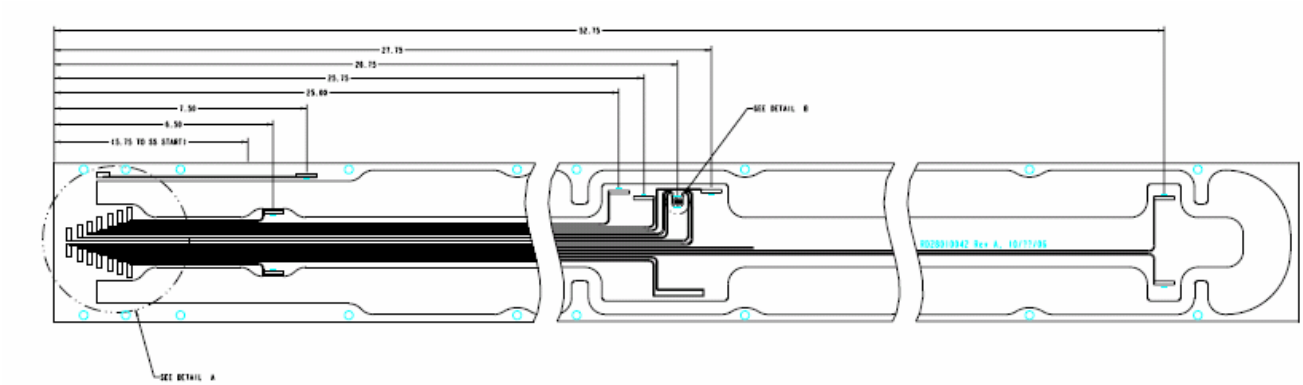

Fig 7.4. Geometry of the LRS01 quench protection heater and flexible circuit.

Two independent circuits, each with four of these strips and its own pulsed power supply, will provide redundancy. In this way, even if there is a failure of one whole circuit, each coil pair would still be quenched on both the inner and outer surfaces. The total resistance of the four strips in a circuit, if connected in series, would be12.4 Ω. To supply up to 100 A through the series heater, the firing circuit would have to supply 1240 V. Providing this much voltage is undesirable, so the four strips can be connected in parallel, and this results in an equivalent resistance for the circuit of 0.775 Ω. This would lower the voltage requirement for 100A through each strip to 310 V. If needed, there also exists the capability of configuring four independent heater circuits with four power supplies.

It can be shown by studying quench protection heater results from the 16 T Nb_3Sn HD1 dipole tests at LBL [7.5], and from the Nb_3Sn HFDA06 dipole and Nb_3Sn TQC01 quadrupole tests at FNAL [7.6], that sufficient surface power density, and therefore quench energy, can be achieved with less than 50 A with the configuration described above. For each narrow heater section of 1 cm width, with a calculated resistance of 0.14 Ω, the surface power delivered with 100 A is 280 W/cm^2. To achieve a minimum required surface power of 50 W/ cm^2 [7.7], the required current would be 42.3 A. In this case, the strip heater power supply would have to provide 169.2 A and 131.13 V (with the four strips configured in parallel). From these considerations, it can be seen that even without any copper shunting, the stainless steel strips in parallel with the described cutout heater sections will provide more than enough power density to quench the coils. Also, as mentioned previously, there is the option of configuring four independent circuits of two strips each with independent power supplies. This would increase the current delivery to the strips by twice.

Regarding the issue of the thermal diffusion time delay, which depends on the amount and type of insulation between the heater strip and the cable, a quench initiated by a strip heater must start by a minimum time after detection of the spontaneous quench and triggering of the strip heater firing circuit. That minimum time has been recommended to be 10ms [7.7]. In Figure 7.5, time delay data taken during quench protection heater tests of the magnet TQC01 at FNAL [7.8] is plotted against heater voltage. It can be seen that a heater voltage of 400V was sufficient to quench the coils with a delay of 10 ms (at 62% I_{ss}, where the hot spot temperature is close to or at peak value), and by 35 ms (at 23% I_{ss}). Assuming a strip heater resistance of 17.5 Ω [7.7], the power density in this case was 40 W/cm^2. It should be noted that the thickness of the Kapton insulation in the TQC01 instrument trace is 0.0254 mm (0.001”). The thickness chosen for LRS01 is twice that, 0.0508 mm (0.002”) in order to decrease the risk of shorts during assembly. The cable fiberglass insulation sleeve will be the same in LRS01 as it was in TQC01. So the insulation between the heater and cable in TQC01 is less by 0.0254 mm (0.001”) of Kapton. This means that, in order to achieve the same delay of 10 ms in as seen in TQC01, a power density of 80 W/cm^2 will be required. This is well within the capabilities of the

LRS01 strip heater scheme already described. For each heater section, the power density delivered at 100A of current is calculated to be 283 W/cm^2, 354% higher than required. This allows for plenty of margin, along with the possibility of providing greater than 100A if necessary.

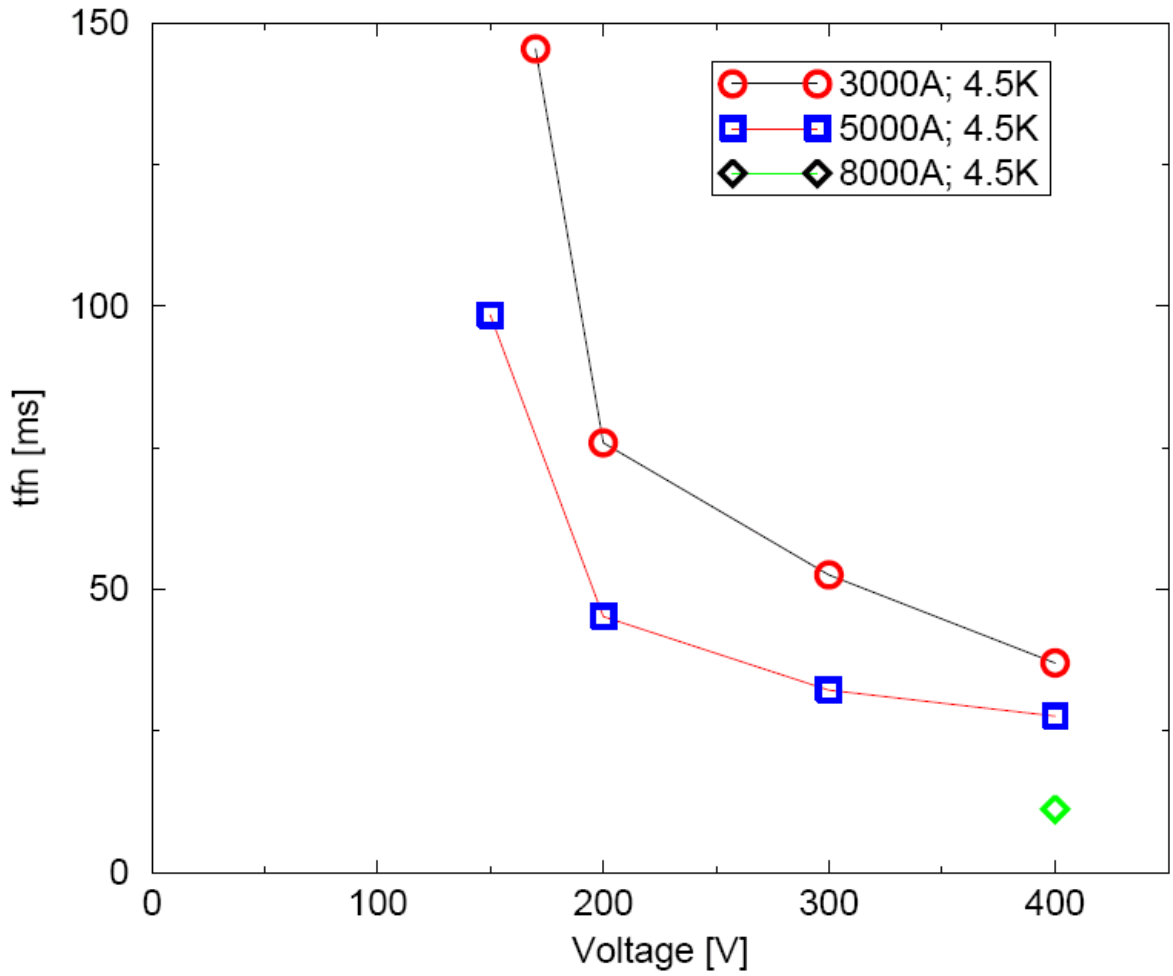

Fig 7.5. Plot of thermal diffusion time delay vs heater voltage for TQC01 protection heater tests.

It should be noted that addition of copper shunting to the stainless steel strips has been common practice in protection heater design. Copper is added either by plating or lamination to the stainless steel in order to lower the total resistive load to the heater power supply and help concentrate power density at selected locations to facilitate fast and adequate heating to the cable.

Though the addition of copper shunting to the stainless steel strips would have these desired effects, there are also introduced some disadvantages. One of these is the issue of skin effect in the copper [7.7]. Also, the lamination process of applying the copper to a flexible circuit is not foolproof and has in the past resulted in variable resistances of the strips due to inadequate bonding. Adding an extra layer to the flexible circuit in order to provide copper bypass would increase coil size and possibly make it difficult to place the coil in the support structure. Also, fabrication of the flexible circuit would be more difficult. Since the power density, time delay, and resistance requirements have

been met by the heater design without copper as described, it was decided that it was not necessary to add copper shunting to the strips.

In addition, energy delivered by the heater can be concentrated in less or more time by varying the time constant of the heater pulse with a capacitor bank consisting of 15 3100 μF capacitors, for a maximum capacitance of 46,500 μF. A schematic sketch of the firing circuit with capacitor bank is shown in Figure 7.6.

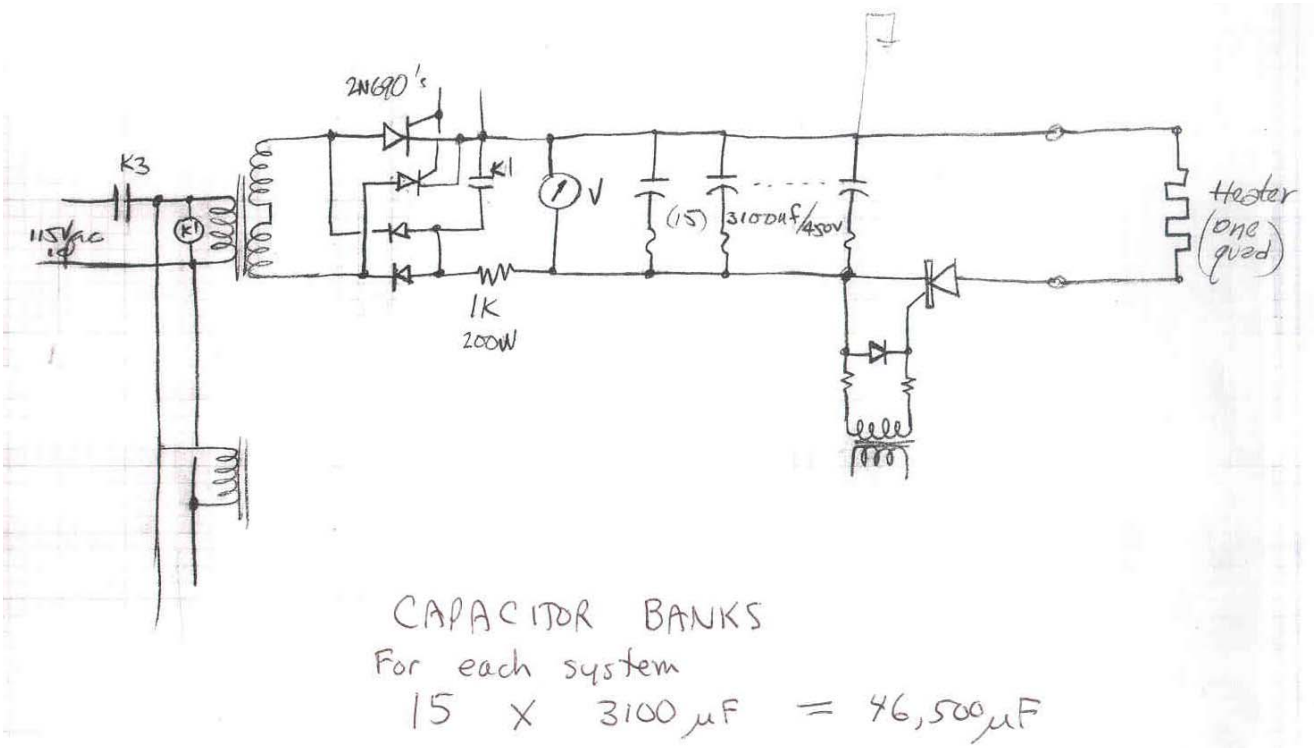

Fig 7.6. Schematic of the quench protection heater firing circuit.

The energy extraction system and the quench protection heaters will both be triggered by pulses from the quench detection circuitry. Quench detection will be accomplished in two ways. One quench detector will look at the voltage difference between the two coil half signals during a quench and will trip when a preset threshold voltage is reached. The other quench detector will likewise look at a voltage difference, here the total coil voltage bucked with the voltage generated by the current derivative. This second quench detector will insure quench detection in the event that the two coil halves quench simultaneously. Final quench detector voltage thresholds are determined during pre-test electrical checkouts. Delays between quench detection and the triggering of the quench protection systems and the power supply shutoff are designed to be at minimum value to decrease further the quench temperatures achieved during quenches.

Both of the quench protection methods described in this section have been used successfully on superconducting magnets tested at BNL, LBL, and FNAL for the SSC, RHIC, and LHC projects and there is a great deal of experience in their use. Recently, quench protection heaters were used effectively on a similar Nb_3Sn racetrack-style 10T common coil dipole at BNL[7.9].

8. COIL INSTRUMENTATION

Goals and descriptions of coil instrumentation are presented in the following list. Voltage tap numbers refer to figure 8.1.

a. Voltage taps on each coil:

Goal: to check if quench origin is in the high field region
- 2 VTs (on turns 10 and 15) on the inner layer of each coil (V_A3 and V_A8)

Goal: to check if quench origin is in the layer jump
- 2 VTs at beginning and end of the layer jump of each coil (V_A10 and V_B10)

Goal: to check if quench origin is in the innermost turn in the ends
- 1 VT on the innermost turn of both layers close to the return end (V_A9 and V_B9)
- note: the lead end is covered by the VTs for the layer jump

Goal: to check if quench origin is in the straight section of the innermost turn
- 1 VT on the innermost turn of each layer close to turn jump (lead end) (V_A11 and V_B11)
- note: the non-lead side is covered by the VT for the layer jump

Goal: to check if quench origin is in the outermost turn of each layer
- 1 VT at the beginning of each outermost turn of each layer (V_A5 and V_B8)

Goal: measure splice resistance
- 2 VTs for each splice (V_A1 - V_A2, and V_B5 – V_B6)

Goal: for magnet protection and quench protection study (hot spot temperature, and quench propagation velocity measurement)
- 1 Spot Heater on turn 12, lead-side, inner layer of each coil
- 2 VTs on turn 12, lead-side, inner layer of each coil at +/- 2.5 cm from the spot heater (V_A6 and V_A7), and 1 VT at 0.5 m from the spot heater (V_A12).

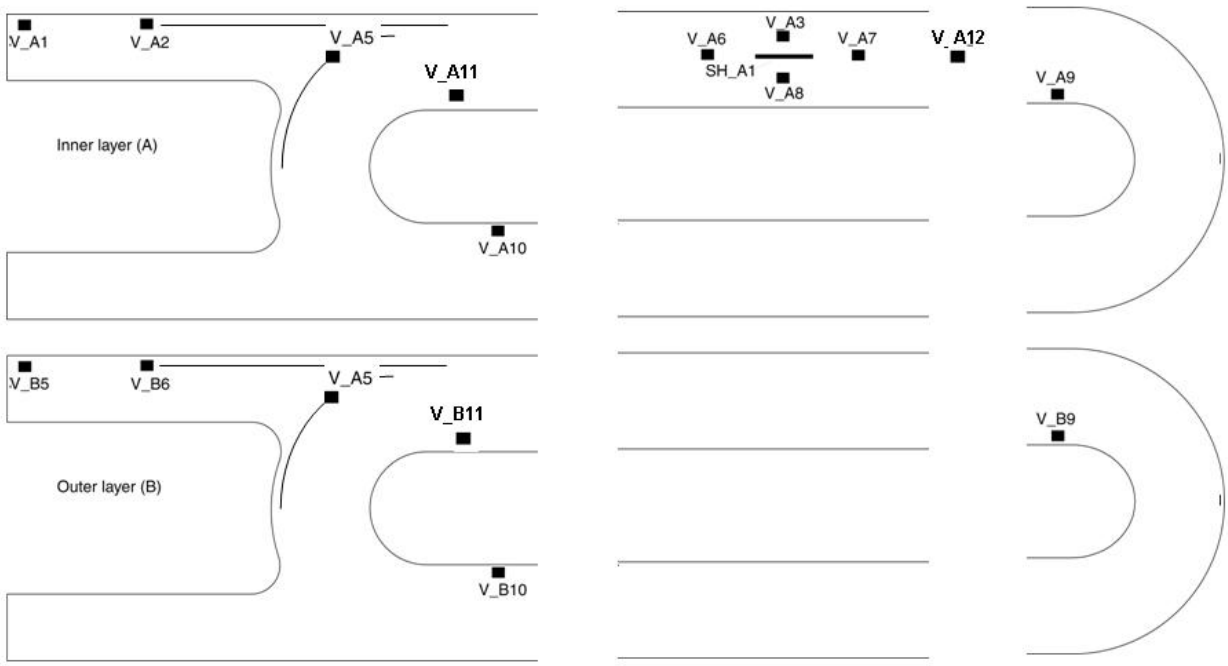

Fig 8.1. Coil instrumentation: voltage taps on inner and outer layer

b. Strain gauge on pole tip

Goal: to check if the pole tip is under compression after cooldown and if it remains under compression during magnet energization.

- 1 Strain Gauge on the pole tip in the return end (only one gauge per coil)

Note: the use of a strain gauge in this location is a new feature never tried before on small racetracks. It will require a special care during coil fabrication in order to avoid excessive transverse load on this gauge when the coil will be installed into the supporting structure, and it's not yet clear if the use of this gauge is compatible with the present design of the pole. Therefore the use of this gauge is still under discussion.

References:

1.1 Hafalia, R.R.; Caspi, S.; Chiesa, L.; Coccoli, M.; Dietderich, D.R.; Gourlay, S.A.; Lietzke, A.F.; O'Neill, J.W.; Sabbi, G.; Scanlan, R.M. "An approach for faster high field magnet technology development;"Applied Superconductivity, IEEE Transactions on Volume 13, Issue 2, Part 2, June 2003 Page(s):1258 - 1261

1.2 Chiesa, L.; Caspi, S.; Coccoli, M.; Dietderich, D.R.; Ferracin, P.; Gourlay, S.A.; Hafalia, R.R.; Lietzke, A.F.; McInturff, A.D.; Sabbi, G.; Scanlan, R.M.; "Performance comparison of Nb/sub 3/Sn magnets at LBNL"Applied Superconductivity, IEEE Transactions on Volume 13, Issue 2, Part 2, June 2003 Page(s):1254 - 1257

7.1 W. Hassenzahl, "QUENCHS Users Manual", Advanced Energy Analysis, Piedmont CA, June, 2005.
7.2 M. Wilson, "Superconducting Magnets", Oxford University Press, 1983.
7.3 L. Imbasciatti, "Studies of Quench Protection in Nb_3Sn Superconducting Magnets for Future Partical Accelerators", PhD Thesis 2003 and Fermilab Technical Division Note TD-03-028.
7.4 B. Bordini, *et al.*, "SQ01b Test Summary", Fermilab Technical Division Note *TD-05-017*, January 2005.
7.5 A. Lietzke, LBL, private communication and unpublished data.
7.6 G. Ambrosio, FNAL, private communication and unpublished data.
7.7 A. McInturff, Texas A&M University, private communication.
7.8 Plot courtesy of S. Feher, FNAL.
7.9 P. Wanderer et al, "Construction and Test of Nb_3Sn Common Coil Magnet DCC017", BNL Magnet Division Note 644-33, Brookhaven National Laboratory, March, 2006.